Materials Today Bio 32 (2025) 101792

Contents lists available at ScienceDirect

Materials Today Bio

journal homepage: www.journals.elsevier.com/materials-today-bio

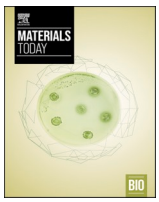

Inhibiting synovial inflammation and promoting cartilage repair in rheumatoid arthritis using a matrix metalloproteinase-binding hydrogel

Zhanpeng Xue [a], Nan Li [a], Kaijun Du [a], Jianxiong Shu [a], Zhenwen Huang [a], Zhifei Gao [b], Xiaobo Xie [a,*], Qi Li [a,**], Yao Lu [a,b,c,***]

[a] Department of Joint and Orthopedics, Orthopedic Center, Zhujiang Hospital, Southern Medical University, Guangzhou, Guangdong, 510282, China
[b] The Second School of Clinical Medicine, Zhujiang Hospital, Southern Medical University, Guangzhou, Guangdong, 510282, China
[c] State Key Laboratory of Multi-organ Injury Prevention and Treatment, Southern Medical University, Guangzhou, Guangdong, 510515, China

ARTICLE INFO

Keywords:
Rheumatoid arthritis
Matrix metalloproteinase-9
Chondroitin sulfate methacrylate
Copper sulfide nanoparticles

ABSTRACT

Originating from synovial tissue, matrix metalloproteinase-9 (MMP-9) is a key inflammatory factor that promotes the formation and invasion of synovial pannus, leading to cartilage matrix destruction in rheumatoid arthritis (RA). However, clinical trials of systemic use of MMP-9 inhibitors are not successful due to severe side effects. Thus, locally inhibiting MMP-9 may be an alternative in the treatment of RA. Herein, we developed MMP-9 binding peptide-functionalized copper sulfide nanoparticles (CuS-T NPs) and delivered them with light cross-linking chondroitin sulfate methacrylate (ChSMA) hydrogel. We found that the CuS NP-doped hydrogels could inhibit synovial inflammation. Specifically, the CuS-T/ChSMA hydrogel could rapidly bind to MMP-9, thereby inhibiting not only the invasion of RA fibroblast-like synoviocytes but also the polarization of inflammatory M1-type macrophages. The underlying mechanism involved the inhibition of the MAPK pathway. Moreover, ChSMA hydrogel provided a cartilage matrix-mimic microenvironment and synergistically promoted the generation of collagen-2 and aggrecan with CuS NPs. In an adjuvant-induced arthritis mouse model, the intra-articular injection of ChSMA/CuS-T hydrogel significantly alleviated synovial inflammation and accelerated cartilage repair without causing any side effects, killing two birds with one stone in RA therapy.

1. Introduction

The formation of inflammatory synovium and pannus usually invades and corrodes the extracellular matrix (ECM) of cartilage in rheumatoid arthritis (RA), the most common autoimmune joint disorder that impacts an estimated incidence of 0.5 %–1 % of the global population [1]. Matrix metalloproteinases (MMPs) are a family of zinc-dependent endopeptidases that play a pivotal role in the degradation of the ECM. Specifically, MMP-9 (gelatinase B), one of the gelatinase subgroups, stands out as a dominator in the progression of cartilage destruction of RA. The primary substrates for MMP-9 include collagen-2 (Col-2) and aggrecan (ACAN), which are the main constituents of cartilage [2]. Predominantly produced by inflammatory macrophages within synovium, MMP-9 activates the growth, migration, and invasion of RA fibroblast-like synoviocytes (RA-FLS) [3]. RA-FLS and macrophages subsequently produce the inflammatory cytokine tumor necrosis factor-α (TNF-α) as the potent inducers of MMP-9 expression [4,5]. The escalating levels of MMP-9 exacerbate the progression of RA, thereby establishing a pernicious cycle [6–8].

To inhibit MMP-9, great efforts have focused on the zinc binding groups (ZBG) within MMP-9 as a target. The first generation of hydroxamic acid drugs, including Batimastat, Marimastat, and GM6001, are designed to bind to the ZBG [9]. However, these drugs face significant challenges: first, the nonselective inhibition of a disintegrin and metalloproteinases (ADAMs) causes severe side effects such as musculoskeletal syndrome in clinical trials; second, the poor solubility and low bioavailability hinder their efficacy. Subsequent iterations, such as Prinomastat and Rebimastat [10], are refined versions of the ZBG

This article is part of a special issue entitled: Multiscale Composites published in Materials Today Bio.

* Corresponding author.
** Corresponding author.
*** Corresponding author. Department of Joint and Orthopedics, Orthopedic Center, Zhujiang Hospital, Southern Medical University, Guangzhou, Guangdong, 510282, China.
E-mail addresses: xilubi@foxmail.com (X. Xie), qili565@foxmail.com (Q. Li), oayul@smu.edu.cn (Y. Lu).

https://doi.org/10.1016/j.mtbio.2025.101792
Received 25 February 2025; Received in revised form 11 April 2025; Accepted 22 April 2025
Available online 23 April 2025

inhibitors, yet they have been withdrawn from clinical trials due to insufficient efficacy and alarming toxicities. The most recent product Minocycline, a derivative of doxycycline, has demonstrated the ability to inhibit MMP-9. However, the concentration required for effective MMP-9 inhibition exceeds the systemic toxic threshold, presenting a significant obstacle [11,12].

Intra-articular injection is a clinical routine in the treatment of arthritis because it can directly target the affected joints [13,14]. Compared to traditional oral or intravenous administration, intra-articular delivery increases drug concentrations in synovial fluid while reducing the incidence of systemic side effects [15]. However, free drug injection is associated with a burst release effect, resulting in a short duration of efficacy and requiring frequent injections. Hydrogels offer the advantages of tunable physical properties, joint lubrication, and sustained slow release of drugs [16,17], making them ideal intra-articular drug delivery systems. In recent years, light crosslinking hydrogels based on methacrylated natural polymers, for example gelatin methacrylate (GelMA), have gained growing attraction in regenerative medicine due to its excellent biocompatibility and ease of operation [18]. When combined with methacrylate (MA) and photoinitiator, these hydrogels provide a stable framework with controlled release and injectable property after a light-driven crosslinking process [19]. Among the methacrylated natural polymers, chondroitin sulfate (ChS) is a type of glycosaminoglycan widely distributed in the ECM and has been approved for the treatment of arthritis [20]. ChS also has a natural affinity for cartilage, favoring the retention of hydrogels at the cartilage injury site [21–23]. However, hydrogel itself is limited by the weak mechanical strength and lack of a regeneration-inducing ability, making it difficult to meet the needs of tissue repair [24,25]. Hence, hydrogel always combine with other materials (e.g., functional nanomaterials) to enhance its mechanical strength and biological activity.

To this end, here we developed peptide functionalized copper sulfide (CuS) nanoparticles (NPs) as therapeutic agents and deliver them using chondroitin sulfate methacrylate (ChSMA) hydrogel. Our previous experiences showed that Cu-based NPs could promote cartilage regeneration in both animal models [26–28] and human cartilage explants [29]. We modified CuS NPs with a cyclic MMP-9-binding peptide (cTTHWGFTLc, designate T) that discovered by phage display [30] to achieve the local inhibition of MMP-9. We found that ChSMA/CuS hydrogel alone could inhibit the invasion of RA-FLS and the polarization of M1-type macrophages. These anti-inflammatory effects were further boosted by ChSMA/CuS-T hydrogel due to their ability to rapidly bind free MMP-9. In an adjuvant-induced arthritis (AIA) mouse model, the intra-articular injection of ChSMA/CuS-T hydrogel significantly suppressed synovial inflammation and protected cartilage, showing potential in RA treatment (Scheme 1).

2. Materials and methods

2.1. Preparation of CuS-T NPs

CuS NPs were synthesized following our reported method [26]. $CuSO_4{\cdot}5H_2O$, L-cysteine, and $Na_2S_2O_3$ was added to 200 mL double distilled water in the mole ratio of 1:3:3. The mixture was magnetically stirred at 500 rpm and heated to 90 °C for 2 h to form the CuS NPs. Then CuS NPs (25 μg mL^{-1}) were mixed with polyacrylic acid (PAA) under magnetic stirring for 4 h for the modification with carboxy groups.

To functionalize with peptide, the cTTHWGFTLc peptide (peptide T) was synthesized from the C′ to the N′ end of the chain by a standard solid phase peptide synthesis (SPPS) method and purified by using reverse-phase high performance liquid chromatography (HPLC). The C' end of the peptide was added with an NH_2-rich linker (GGGKKK) to facilitate the crosslinking of the peptide with CuS-COOH NPs. Finally, CuS-T NPs (NP: peptide = 10:1) were obtained though a classic 1-(3-

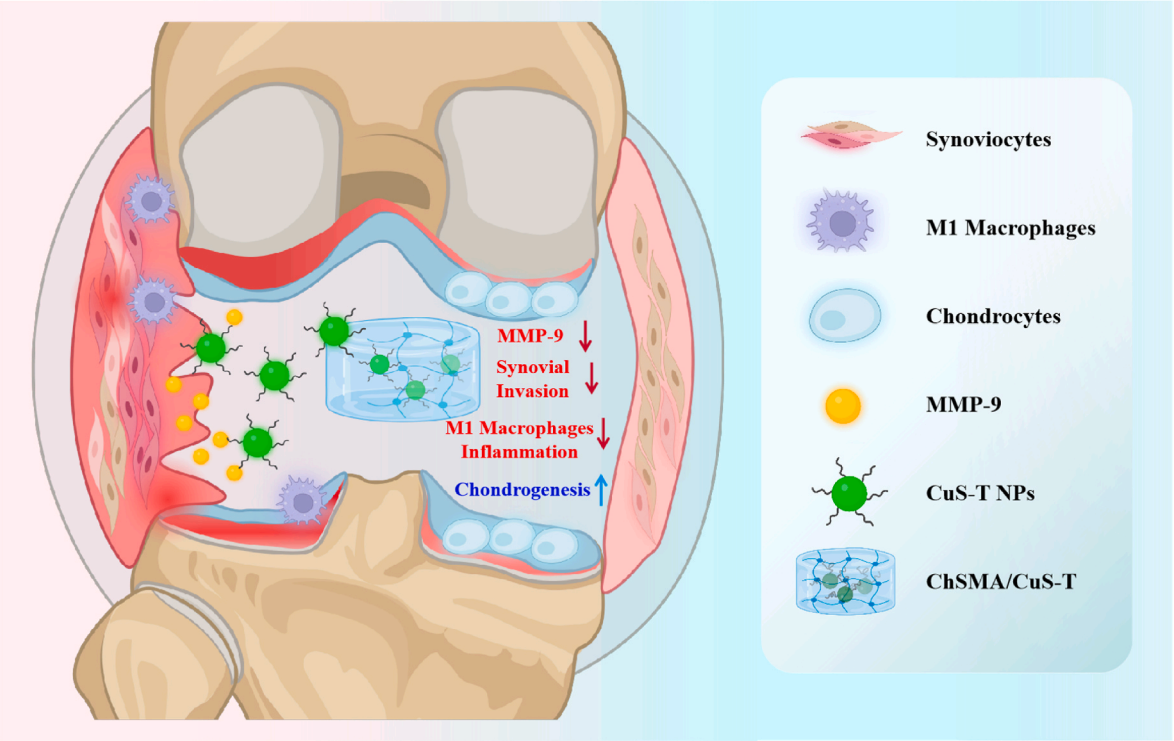

Scheme 1. Illustration of the application of ChSMA/CuS-T hydrogel in RA therapy. The inflammatory M1 type macrophages and synoviocytes release MMP-9 and cytokines to erose articular cartilage in RA. The ChSMA/CuS-T hydrogel can not only rapidly bind MMP-9 but also inhibit the invasion of synoviocytes as well as polarization of M1 macrophages. The hydrogel also exhibits strong chondroinductivity due to the presence of CuS NPs and chondroitin sulfate even under inflammatory microenvironment. Hence, intra-articular injection of ChSMA/CuS-T hydrogel alleviates joint inflammation and promotes cartilage regeneration, achieving an efficient RA therapy.

Dimethylaminopropyl)-3-ethylcarbodiimide (EDC; 25 μg mL^{-1})/N-Hydroxysuccinimide (NHS; 25 μg mL^{-1}) reaction.

2.2. Preparation of ChSMA/CuS-T hydrogel

ChSMA was synthesized using the method reported with modifications [31]. ChS (Macklin Inc., China) was dissolved in 1.0 M phosphate-buffered saline (PBS) at a concentration of 0.2 g mL^{-1}. Subsequently, MA dissolved in dimethyl sulfoxide (DMSO) was added to the ChS solution over a period of 30 min in a volumetric ratio of 0.06: 1. After a 2-h reaction, the pH of the mixture was adjusted to 10 using 5 M sodium hydroxide, and the reaction was allowed to proceed for an additional 22 h. The mixture was then dialyzed against double distilled water using a 3.5 kDa dialysis membrane for 12 h, and the dialyzed ChSMA solution was lyophilized.

To prepare the hydrogels, ChSMA was dissolved in a lithium phenyl (2,4,6-trimethylbenzoyl) phosphinate (LAP) solution at a 5 % weight/volume concentration. CuS-T or CuS NPs were added into the ChSMA/LAP solution. The mixture was crosslinked under 405 nm light for 30 s to form the hydrogels. Pure ChSMA hydrogel were also prepared followed the same methods but without adding NPs. For in vitro study, the hydrogel extractions were prepared by soaking different hydrogels in the culture medium for 3 days.

2.3. Characterization of the NPs and hydrogels

The morphology of CuS and CuS-T NPs was observed using transmission electron microscopy (TEM). The hydrodynamic size of CuS and CuS-T NPs was analyzed by dynamic light scattering (DLS). Zeta potentials and absorption spectra of CuS, CuS-COOH, and CuS-T NPs were detected. The morphology of ChSMA, ChSMA/CuS, and ChSMA/CuS-T hydrogels was examined using scanning electron microscopy (SEM) and TEM. After freeze-drying, the hydrogels were coated with gold, and examined with SEM. For TEM analysis, the hydrogels were treated with liquid nitrogen, ground into powder, and suspended in ethanol. Then a drop of the suspension was placed onto a carbon-coated copper grid and the morphology was studied by TEM. The rheological properties of the hydrogels were assessed using the Haake Mars40 system with parameters of frequency 1 Hz, strain 1 %, amplitude 0.5 %, and region 0.1–100 rad/s. To detect the release of Cu ions, the ChSMA/CuS-T hydrogel was incubated in the simulated body fluid at 37 °C, and the supernatant were collected on day 1, 2, 3, 5, and 7. Then ICP-MS was conducted to detect the content of Cu ions. To assess whether the hydrogels can bind MMP-9, 50 μL of ChSMA, ChSMA/CuS, and ChSMA/CuS-T hydrogels were respectively added in the bottom of 96-well plate, and cultured with 150 μL MMP-9 solution (20 ng/mL). Then the free MMP-9 within the culture supernatant was determined using an ELISA kit (MU30613, Bioswamp) following the manufacturer's instructions.

2.4. Cytotoxicity and hemolytic test

Mice bone marrow mesenchymal stem cells (BMSCs; MUBMX-01001, Cyagen) were used to examine in vitro cytotoxicity. BMSCs were seeded in 96-well plate and cultured with normal medium or the hydrogel extractions for 24, 48, and 72 h. Cell viability was investigated by a cell counting kit 8 (CCK-8; BMU106, Abbkine). Live/death staining was also performed to verify the cytotoxicity of hydrogels. For hemolytic test, fresh mice blood was collected and diluted with PBS (4:5 by volume). The diluted blood (200 μL) was incubated with 1 mL of PBS, double distilled water, or the hydrogels for 1 h, respectively. All samples were centrifuged, and then the optical density value (O.D.) of the supernatants was measured at 545 nm and the hemolysis ratio was calculated.

2.5. Cell migration and invasion in vitro

Cell migration was conducted using a wound-healing assay. Specifically, 5×10^5 RA-FLS (JNO-H0336, Jennio-bio, China) were seeded in a 6-well plate and cultured with various hydrogel extracts (ChSMA, ChSMA/CuS, ChSMA/CuS-T) or normal medium. A straight scratch was introduced perpendicularly across the cell monolayer. Images were captured using a bright field microscope at 24 and 48 h. The reduction in scratch area was calculated and quantified. The cell invasion assay was investigated utilizing a transwell system. 2×10^4 RA-FLS were seeded into the upper chamber and cultured with serum-free hydrogel extracts or normal medium, and the lower chamber was filled with complete medium containing 10 % fetal bovine serum. After a 24-h incubation, the upper chamber was removed, washed, and stained with crystal violet. The invaded cells were then observed and counted under a bright field microscope.

2.6. Anti-inflammation effect of the hydrogels in vitro

Mouse macrophages cell line RAW264.7 cells (iCell Bioscience Inc, Shanghai, China) were induced by lipopolysaccharides (LPS) at a concentration of 250 ng mL^{-1} to establish an in vitro proinflammatory cellular model. RAW264.7 cells (blank control) or LPS-induced RAW264.7 cells were cultured with various conditional media for an additional 24 h: 1) complete medium without LPS as the blank group; 2) complete medium with LPS as the control group; 3) ChSMA extracts with LPS; 4) ChSMA/CuS extracts with LPS; and 5) ChSMA/CuS-T extracts with LPS.

For real-time polymerase chain reaction (RT-qPCR) analysis, RNA was extracted, followed by the synthesis of complementary DNA (cDNA) using reverse transcription reagents. The relative mRNA expression levels of *TNF-α* and *MMP-9* were normalized to *GAPDH* and quantified using SYBR reagent on a LightCycler®480 II. The primers used in RT-qPCR are listed in Table S1 (Supporting Information).

Immunofluorescence (IF) analysis was conducted on RAW264.7 cells seeded in confocal dishes. After incubation, cells were fixed with 4 % paraformaldehyde for 30 min and blocked with QuickBlock™ Blocking Buffer for Immunofluorescence Staining (P0260, Beyotime) for 15 min. Then they were incubated with primary antibodies against MMP-9 (ET1704-69-100, HUABIO) and TNF-α (ER65189, HUABIO) at 4 °C for 12 h. Following a 1-h incubation at room temperature with secondary antibodies, immunofluorescence images were captured using a confocal immunofluorescence microscopy.

2.7. Anti-inflammation mechanism of ChSMA/CuS-T hydrogel in vitro

To study the mechanism underlying the anti-inflammation effect of hydrogels, we cultured LPS-induced RAW264.7 cells with normal medium or ChSMA/CuS-T extracts for 24 h, and then transcriptome analysis was performed [28,32]. Total RNA was extracted from cells using TRIzol Reagent. An Agilent 2100 BioAnalyzer and Qubit RNA assay kits were used to measure the quality and quantity of RNA, respectively. mRNA libraries were generated using Illumina HiSeq X10. Gene expression levels were determined using RSEM v1.2.28 and normalized by using the trimmed mean of M-values. Differentially expressed genes (DEGs) were identified using edgeR software. DEGs showing altered expression with $P < 0.05$ and more than 1.5-fold changes were selected. To investigate DEGs enriched in signaling pathways, Gene Ontology (GO) and Kyoto Encyclopedia of Genes and Genomes (KEGG) pathway enrichment analysis was conducted in the downregulated DEGs.

2.8. Chondrogenic inductivity of the hydrogels in vitro

Different hydrogels were immersed in mouse BMSCs chondrogenic differentiation medium (MUXMX-90041, Cyagen) for 3 days to obtain chondroinductive extracts. For RT-qPCR, BMSCs were seeded into a 6-

well plate and cultured with the chondroinductive extracts for 5 days. The expression levels of *Col-2*, *ACAN* and SRY-box transcription factor 9 (*SOX9*) were quantified.

To form cell pellets, 5×10^5 BMSCs was centrifuged in 10 mL conical bottom tubes. Cell pellets were cultured with chondroinductive extracts. After 28 days, cell pellets were collected, fixed by 4 % paraformaldehyde, embedded in agar, sectioned, and performed IHC staining of Col-2 and ACAN.

2.9. Interactions between RAW264.7 cells and BMSCs

The culture supernatant of LPS-induced RAW264.7 cells was collected to obtain the inflammatory conditional media. The inflammatory conditional media were mixed with different chondrogenic extracts in a ratio of 1:9 by volume for the culture of BMSCs. After a 5-day culture, RNA was extracted from the BMSCs and the relative mRNA expression levels of *Col-2*, *ACAN*, and *SOX9* were quantified by RT-qPCR.

2.10. Establishment of an AIA mouse model

We established an AIA mouse model followed our previously reported method [33,34] for in vivo study of the hydrogels. All animal experiments and procedures were approved by the Ethics Committee of the Laboratory Animal Center of Zhujiang Hospital, Southern Medical University (LAEC-2023-094). 6 weeks old C57BL/6J mice were purchased from Zhuhai BesTest Bio-Tech Co., Ltd, China. For initial immunization, a total of 150 μL of complete Freund's adjuvant (F5881 Sigma-Aldrich) was injected into bilateral armpits and hind paw pads of each mouse. After one week, 10 μL of incomplete Freund's adjuvant (F5506 Sigma-Aldrich) was injected into right knee cavity of each mouse for the booster immunization. After an additional 1 week, the AIA model was successfully established.

2.11. In vivo therapeutic effect and safety of the hydrogels

The AIA mice were randomly divided into four groups (n = 5 each group) and treated as followed: 1) PBS; 2) ChSMA; 3) ChSMA/CuS; and 4) ChSMA/CuS-T (20 μL). The hydrogels were administered via intra-articular injection into the right knee cavity once a week for 4 weeks. The patellar ligament and joint capsule of the right knee was exposed, and then different formulations were injected into knee cavity using an insulin syringe. Finally, the joint was irradiated with a 405 nm light for 30 s to achieve gelation in situ. After different treatments, gait analysis of mice was performed using the Noldus CatWalk XT gait analysis system.

The right knee joints and major organs, including heart, liver, spleen, lung, and kidney were collected. Blood serum was acquired and underwent biochemical tests using the Biochemical Analyzer (BS-240VET, Mindray) and Hematology Analyzer (SX-350001594A, Mindray). Hematoxylin-eosin (H&E) staining was performed on the organ sections.

The right knee joints of mice were fixed by 4 % paraformaldehyde, decalcified for 2 weeks, embedded by paraffin, and sectioned. H&E and Safranine O-fast green staining were performed. After antigen retrieval by Pepsin Antigen Retrieval Solution (X1035, Solarbio) and blocked by QuickBlock™ Blocking Buffer for Immunol Staining (P0260, Beyotim), sections were incubated with primary antibody of MMP-9 (ET1704-69-100, HUABIO), TNF-α (ER65189, HUABIO), Col-2 (ab308455, ABCAM), and ACAN (bs-1223R, BIOSS) at 4 °C for 12 h. All primary antibody were diluted by 1:100. After an additional 1 h at room temperature for secondary antibody incubation, the IHC image was taken under a high-content fluorescence microscopy.

In addition, 20 μL of Cy5.5-labeled ChSMA/CuS-T hydrogel was injected intraarticularly to study the in vivo degradation. At days 1, 4, and 7, mice were imaged by a fluorescence imaging system (excitation wavelength: 630 nm, emission wavelength: 700 nm; FX PRO, BRUKER, Germany).

2.12. Statistics analysis

Data were presented as mean ± standard deviation (mean ± SD). Significance was determined using one-way ANOVA followed by Tukey's multiple comparisons test. A *P*-value less than 0.05, 0.01, 0.001 and 0.0001 was regarded as statistically significant with an increasing level of the significance.

3. Results and discussion

3.1. Preparation and characterization of the NPs and hydrogels

CuS NPs were chemically synthesized and present a spherical shape with a size of ~100 nm (confirmed by TEM; Fig. 1b). We then modified CuS NPs with –COOH by PAA to facilitate the conjugation of $–NH_2$-rich MMP-9-binding peptide. The zeta potentials of CuS and CuS-PAA NPs were approximately −10.0 and −15.0 mV, respectively (Fig. 1c). PAA, a linear polymer prepared by free radical polymerization of acrylic monomer, is rich in -COOH and carries substantial negative charge after dissociation. CuS-PAA NPs exhibited stronger negative charged relative to CuS NPs after conjugated, indicating the successful modification of –COOH on the NPs. After peptide conjugation, CuS-T displayed a neutral charge of ~1.0 mV. Utilizing a peptide calculator, we determined that the peptide T has an isoelectric point of 9.8 and carries a +3.0 net charge at pH 7 (Fig. S1, Supporting Information). Thus, the increased charge in CuS-T NPs compared to CuS-PAA NPs suggested that the NPs were conjugated with the peptide. This result was further confirmed by the new peak at 230–290 nm in the absorption spectrum of the NPs (Fig. 1d). Moreover, CuS-T NPs showed no obvious changes in morphology and size (as determined by TEM; Fig. 1b). DLS measurement indicated that the hydrodynamic size of CuS NPs was ~150 nm and their average diameter slightly increased to ~200 nm after peptide modification (Fig. S2, Supporting Information).

Then CuS-T NPs were doped into ChSMA/LAP solution and formed the hydrogels upon exposure to 405 nm light (Fig. 1e). CuS-T NPs were observed in the ChSMA/CuS-T hydrogel (as investigated by TEM; Fig. S3, Supporting Information). The SEM images revealed that all hydrogels presented a typical porous structure after freeze-drying (Fig. 1f). Rheological tests of ChSMA/CuS-T hydrogels showed that the storage modulus (G') was higher than the loss modulus (G''), indicating the formation of typical hydrogels in a semi-solid state (Fig. 1g). Moreover, ICP-MS showed that the content of Cu ions in the incubation supernatant increased over time, demonstrating that the NPs could gradually release from the ChSMA/CuS-T hydrogel (Fig. S4, Supporting Information).

Furthermore, the ELISA results confirmed that the content of free MMP-9 in the supernatant of ChSMA/CuS-T group was significantly lower than those in the ChSMA and ChSMA/CuS groups (Fig. 1h). Synovial fluids derived from RA patients contain an elevated level of MMP-9 [35]. The concentration of MMP-9 in synovial fluid is markedly higher in erosive RA compared to non-erosive early-stage RA [36]. Thus, ChSMA/CuS-T hydrogels could indeed bind MMP-9 in RA-related microenvironment, showing the potential of local inhibition of MMP-9.

In addition, we observed the in vivo degradation of ChSMA/CuS-T hydrogel by labeled the hydrogel with Cy5.5. The fluorescence images (Fig. 1i) of joints showed that a strong red fluorescence after intra-articular injection of Cy5.5-labeled ChSMA/CuS-T hydrogel, and then the fluorescence intensity gradually decreased over time. The red fluorescence could be detected for approximately 7 days, suggesting that the hydrogel was stable in vivo.

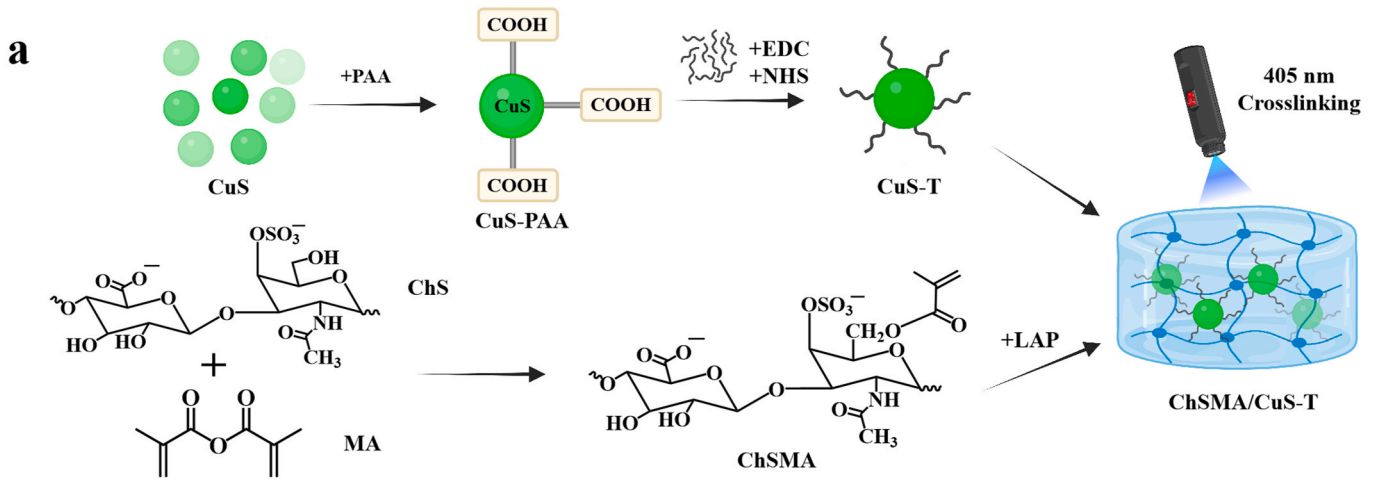

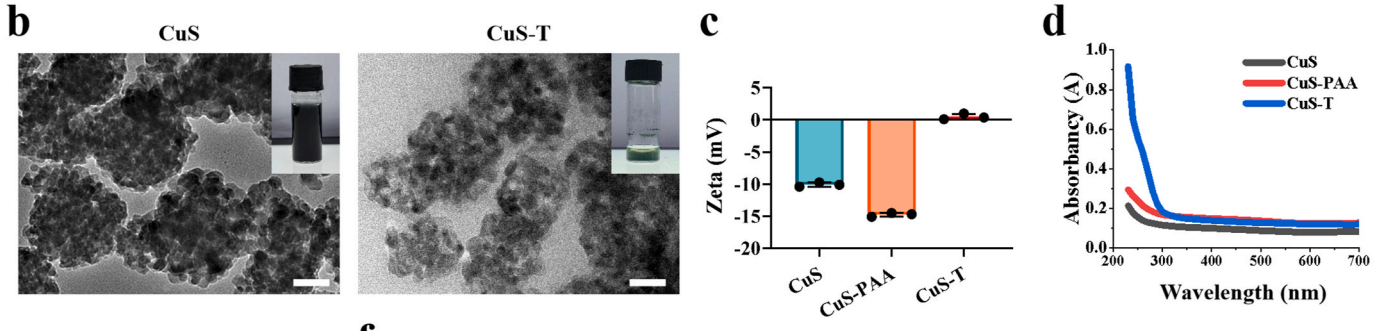

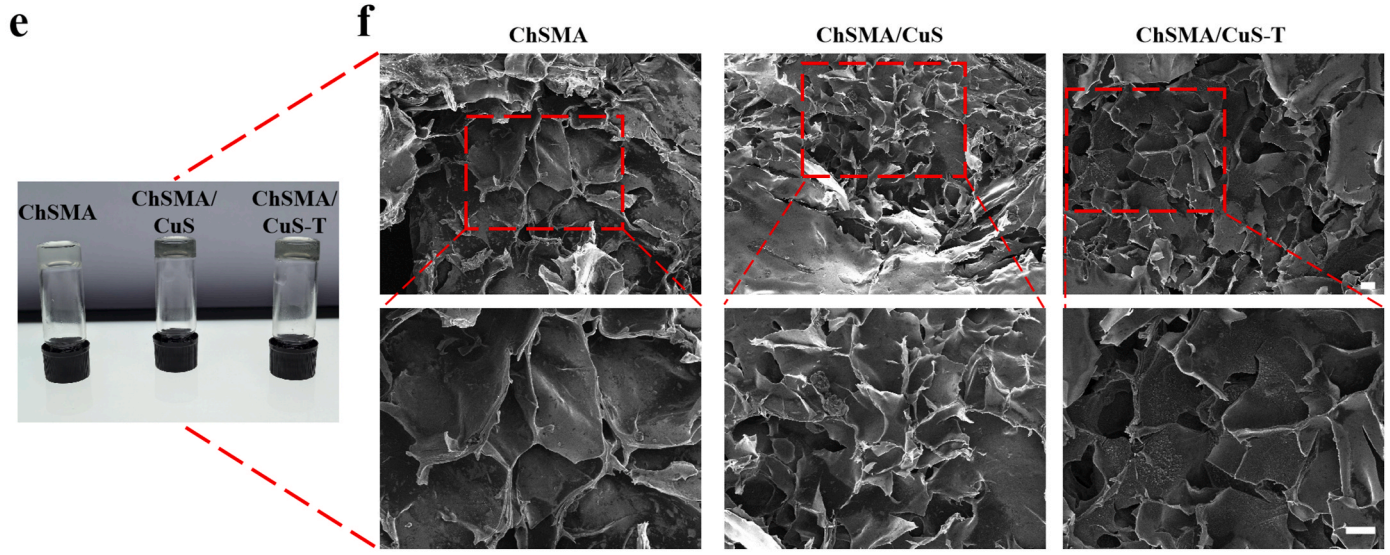

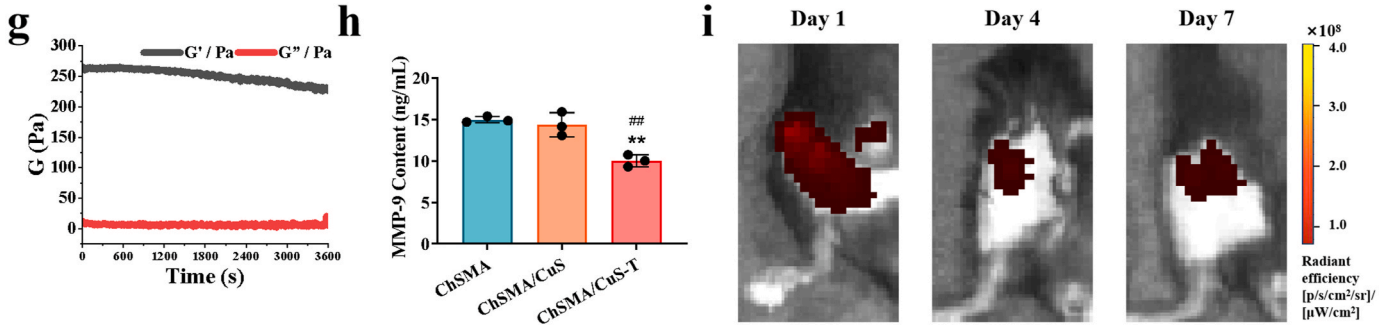

(caption on next page)

Fig. 1. Preparation and characterization of the NPs and hydrogels. (a) Illustration of synthesis of CuS-T NPs and ChSMA/CuS-T hydrogel. CuS NPs were modified with PAA to obtain carboxy groups, and then CuS-PAA NPs were conjugated with NH_2-rich MMP-9-binding peptides (cTTHWGFTLc, termed T) via an EDC/NHS reaction. A mixture of ChSMA/LAP and CuS-T NPs was crosslinked under 405 nm light irradiation for 30 s to form the ChSMA/CuS-T hydrogel. (b) TEM image of CuS and CuS-T NPs. Insert: photo of CuS (40 mg/mL) and CuS-T (1 mg/mL) NP solution. Scale bar = 50 nm. (c) Zeta potentials of CuS, CuS-PAA, and CuS-T NPs. The changes of zeta potentials from negative charge to positive charge suggested the successful conjugation of peptides on the NPs. (d) Absorption spectra of the NPs. A new peak was observed in ChSMA/CuS-T NPs in the range of 230–290 nm after peptide conjugation. (e) Photos of the hydrogels. (f) SEM images showing the porous structure of the hydrogels after freeze-drying. Scale bar = 50 μm. (g) Rheology test of ChSMA/CuS-T hydrogel. (h) ELISA of MMP-9 content in the supernatant. This result indicated that ChSMA/CuS-T hydrogel could bind MMP-9. (i) Fluorescence imaging of mice after intraarticular injection of Cy5.5-labeled ChSMA/CuS-T hydrogel.

3.2. ChSMA/CuS-T hydrogel is safe to BMSCs while inhibits migration and invasion of RA-FLS

Since the hydrogels are degradable and the NPs can release from the hydrogels, we prepared the hydrogel extracts to simulate this process and used them in the in vitro study. We first cultured BMSCs with hydrogel extracts to evaluate the cytotoxicity of the hydrogels. The CCK-8 results indicated that BMSCs proliferated rapidly in all groups during 3 days of culture (Fig. 2a). Live/dead staining (Fig. 2b) also indicated that most cells were alive (green fluorescence) and dead cells (red fluorescence) were negligible. In addition, hemolysis test (Fig. 2c) showed that the supernatant of blood samples was transparent in all hydrogel groups, suggesting that the hydrogels did not damage red blood cells or cause the release of hemoglobin. Hence, ChSMA/CuS-T hydrogel was biocompatible to mammal cells.

Synovial tissue, mainly composed of RA-FLS, undergoes significant hyperplasia, inflammation, and invasiveness in RA, leading to the destruction of cartilage and bone within the affected joints [37,38]. Thus, we conducted wound healing and transwell assays to evaluate the inhibitory effects of our hydrogels on RA-FLS migration and invasion (Fig. 2d and e). Interestingly, we found that both ChSMA/CuS and ChSMA/CuS-T hydrogels significantly impeded the migration of RA-FLS. Notably, approximately 90 % wound closure rate was observed in both the control and ChSMA groups at 48 h, whereas the ChSMA/CuS and ChSMA/CuS-T group maintained a 79 % and 55 % closure rate, respectively (Fig. 2f). The transwell assay results also demonstrated a marked inhibitory effect of both ChSMA/CuS and ChSMA/CuS-T hydrogels on cell invasion. Specifically, ChSMA/CuS-T hydrogel significantly reduced the number of invaded RA-FLS to approximately 10 after a 24-h culture. However, there were approximately 55 cells that invaded into the lower chamber in the control and ChSMA groups (Fig. 2g).

MMP-9 plays a crucial role in activating the growth, migration, and invasive capabilities of RA-FLS [3]. A previous study finds that the proliferation, migration, and autophagy of RA-FLS are modulate through the MMP-9/RAGE/TLR9 axis [39]. Another research reveals that SOX5 can regulate MMP-9 expression and local knockdown of SOX5 in RA model can inhibit FLS migration and invasion through inhibiting MMP-9 expression [40]. Hence, the binding of MMP-9 by ChSMA/CuS-T hydrogel could efficiently inhibit the migration and invasion of RA-FLS.

3.3. ChSMA/CuS-T hydrogel reduces inflammation of M1-type macrophages in vitro

We stimulated RAW264.7 cells with LPS to polarize them into the inflammatory M1 type. A significant upregulation was found in the gene expression of *MMP-9* and *TNF-α* under LPS stimulation. In contrast, the ChSMA, ChSMA/CuS, and ChSMA/CuS-T groups exhibited varying degrees of downregulation of these markers even under continuous LPS stimulation. Notably, the ChSMA/CuS group displayed a pronounced inhibition of *TNF-α* and *MMP-9*, suggesting CuS NPs themselves exhibited the anti-inflammatory property. In the ChSMA/CuS-T group, the level of *MMP-9* have no difference with the blank control group and the level of *TNF-α* was lowest among all treatment groups (Fig. 3a).

We confirmed the protein expression of MMP-9 and TNF-α by IF staining (Fig. 3b and c). Consistent with the RT-qPCR results, IF images showed that RAW264.7 cells exhibited intensified fluorescence intensity in the LPS-induced control group compared to those in the blank group, indicating that M1 type macrophages expressed higher level of MMP-9 and TNF-α. The ChSMA and ChSMA/CuS groups showed a mild level of MMP-9 expression. In contrast, the fluorescence intensity of MMP-9 in M1 macrophages cultured with the ChSMA/CuS-T hydrogel extracts was negligible due to the presence of MMP-9-binding peptide on the surface of CuS-T NPs. As to TNF-α, macrophages in both ChSMA/CuS and ChSMA/CuS-T groups decreased to a normal level akin to the blank group. Thus, the ChSMA/CuS-T hydrogel could not only suppress the expression of MMP-9 but also alleviate the anti-inflammatory activity of M1-type macrophages.

We further conducted transcriptome analysis to explore the mechanism underlying the anti-inflammatory effect of ChSMA/CuS-T hydrogel. Volcano plots showed the genes in RAW264.7 that were differentially expressed between the ChSMA/CuS-T and PBS groups (Fig. 4a). There were 54 significantly upregulated genes and 139 downregulated genes in the ChSMA/CuS-T group compared with the PBS group. KEGG pathway enrichment analysis of the downregulated DEGs revealed that the anti-inflammatory effect of ChSMA/CuS-T hydrogel was highly related to the mitogen-activated protein kinases (MAPK), rat sarcoma virus (Ras), and Ras-related protein 1 (Rap1) signaling pathway (Fig. 4b). The GO analysis (Fig. 4c) revealed a significant downregulation in the ChSMA/CuS-T hydrogel regarding the GTPase activity within biological process and molecular function. This result aligns with the KEGG pathway analysis because Ras and Rap1 are typical GTPases [41]. GSEA analysis (Fig. 4d) further confirm the inhibition of these pathways in the ChSMA/CuS-T hydrogel group.

The MAPK pathway governs a spectrum of cellular activities, including cell growth, proliferation, differentiation, and migration [42]. In RA, the activation of MAPK pathway in macrophages and synovial fibroblasts promotes the secretion of a plethora of pro-inflammatory cytokines such as IL-1β, IL-6, TNF-α, and MMPs while bolstering anti-apoptotic properties [43]. MAKP has complex interactions with other signaling pathways such as NF-κB and Akt/mTOR. For example, the MAPK pathway works collaboratively with the NF-κB pathway to regulate inflammation, while the Akt/mTOR pathway is involved in FLS migration and invasion [44,45]. The inhibition of the Ras-MAPK signaling pathway exerts a suppressive effect on the proliferative activities and apoptotic resistance of RA-FLS [46]. The Ras kinase, serving as the initial catalyst of the ERK-a branch within the MAPK signaling pathway, initiates a sequence of activations starting with the upstream MAPKKK-RAF, proceeding through the midstream MAPKK-MEK, and culminating in the activation of the downstream MAPK-ERK [47]. Rap1, a small GTPase and member of the Ras family of GTPases [48], synergizes with Ras to potentiate the ERK signaling pathway [49]. The activation of ERK1 and ERK2, spurred by the presence of anticitrullinated protein antibodies (ACPA; a specific marker of RA), results in the substantial production of TNF-α by macrophages [50]. Moreover, activated ERK increases the production of cyclooxygenase-2 (COX-2) and prostaglandin E−2 (PGE-2) by RA-FLS, which further promote the production of inflammatory factors, resulting in synovial inflammation and bone destruction [51].

Consequently, the polarized macrophages accompany with inflammatory factors, stimulate the production of MMPs in synovial fibroblasts, leading to the degradation of cartilage and bone, thereby exacerbating RA [52]. Therefore, ChSMA/CuS-T hydrogel mitigated M1

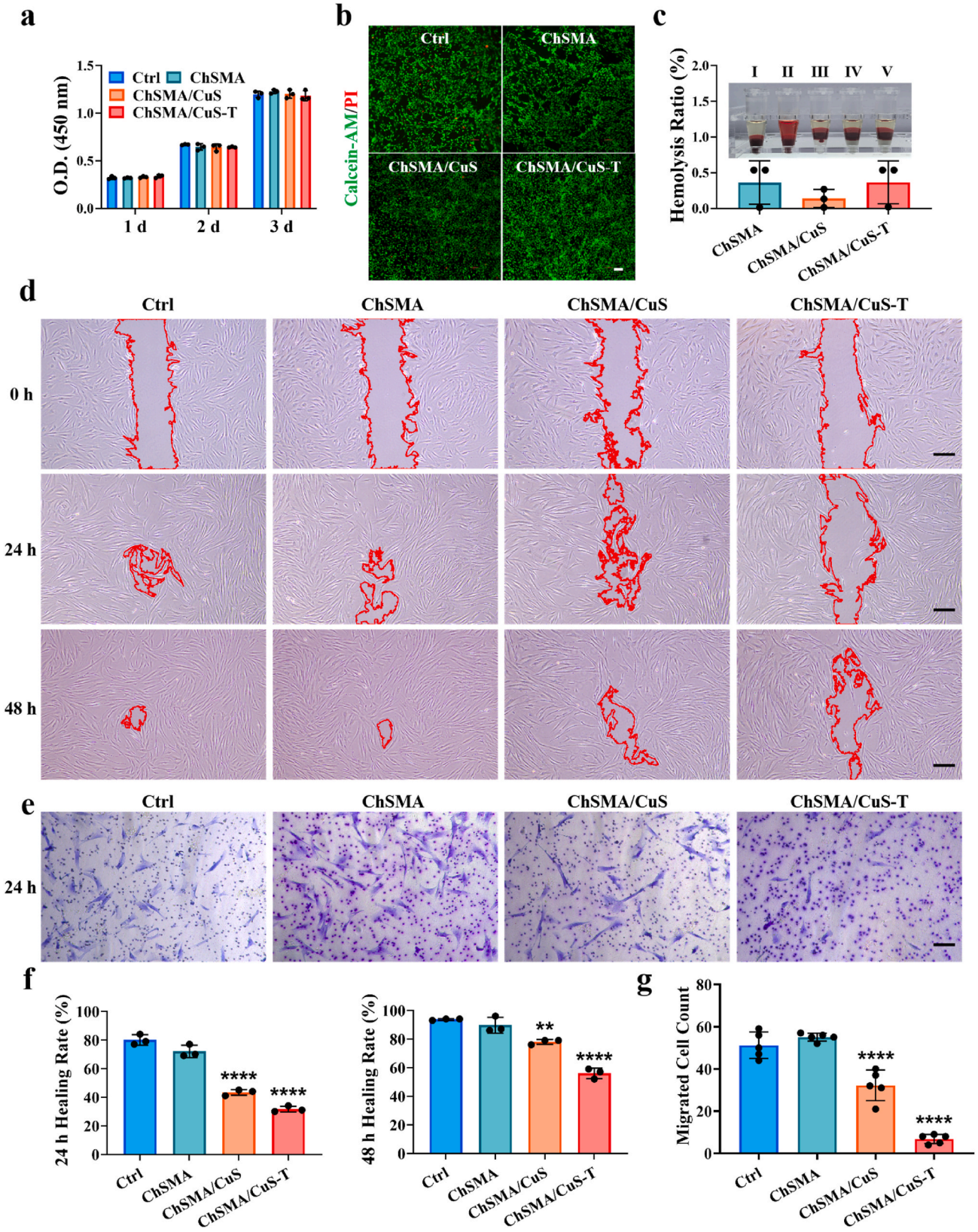

Fig. 2. Cytotoxicity, inhibition of RA-FLS migration and invasion. (a) Cell viability of BMSCs cultured with different hydrogel extracts. (b) Live/dead staining of BMSCs. Scale bar = 100 μm. (c) Hemolysis ratio of the hydrogels. Inset: photo of blood samples after incubated with (I) PBS (negative control), (II) double distilled water (positive control), (III) ChSMA hydrogel, (IV) ChSMA/CuS hydrogel, and (V) ChSMA/CuS-T hydrogel, respectively. (d) Wound healing of RA-FLS treated with different hydrogels. (e) Transwell assay of RA-FLS cultured with the hydrogels. Scale bar = 100 μm. Quantitative analysis of wound healing rate (f) and transwell assay (g). $^{**}P < 0.01$, $^{****}P < 0.0001$, compared with the control group.

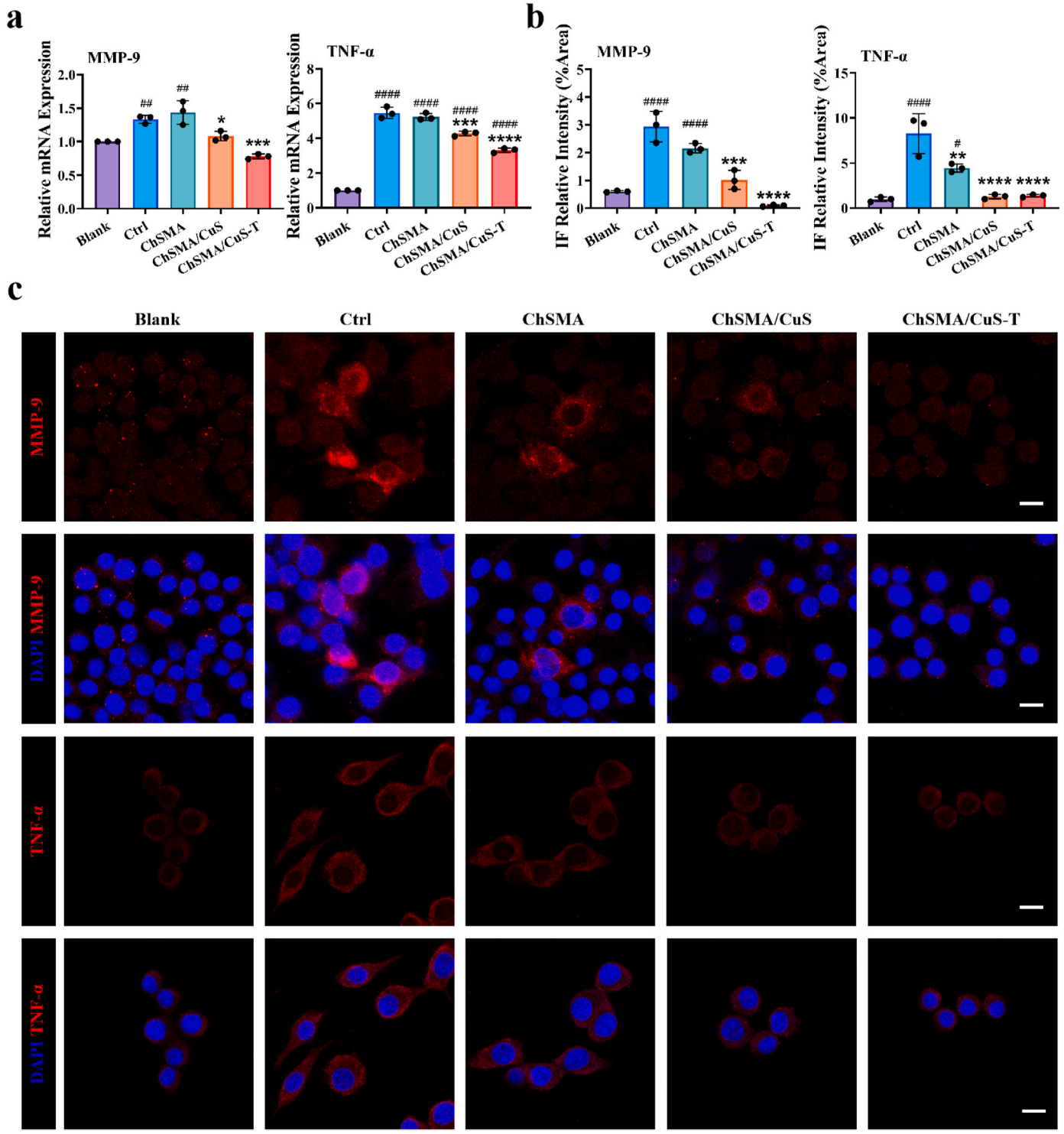

Fig. 3. Anti-inflammatory effect of the hydrogels. (a) Relative gene expression levels of *MMP-9* and *TNF-α* of macrophages after different treatments. RAW264.7 cells without LPS stimulation were served as the blank control. In other groups, RAW264.7 cells were treated with 250 ng/mL LPS to maintain the inflammatory M1 type. (b) Statistical analysis of immunofluorescence intensity derived from panel (c). (c) Fluorescence images of the expression of M1 macrophage markers TNF-α and MMP-9. Scale bar = 25 μm. These results indicated that ChSMA/CuS-T hydrogels could inhibit MMP-9 and TNF-α expressions in M1 type macrophages. $^{*}P < 0.05$, $^{**}P < 0.01$, $^{***}P < 0.001$, $^{****}P < 0.0001$ compared with the control group. $^{\#}P < 0.05$, $^{\#\#}P < 0.01$, $^{\#\#\#\#}P < 0.0001$ compared with the blank group.

macrophage inflammation by downregulating the MAPK signaling pathway where Ras and Rap1 play synergistic roles.

3.4. ChSMA/CuS-T hydrogel promotes chondrogenesis of BMSCs under inflammatory microenvironment

The ChSMA (one of the ECM components) and CuS NPs (favoring chondrogenesis) were expected to cultivate a conducive environment for cartilage repair. Compared with other components of

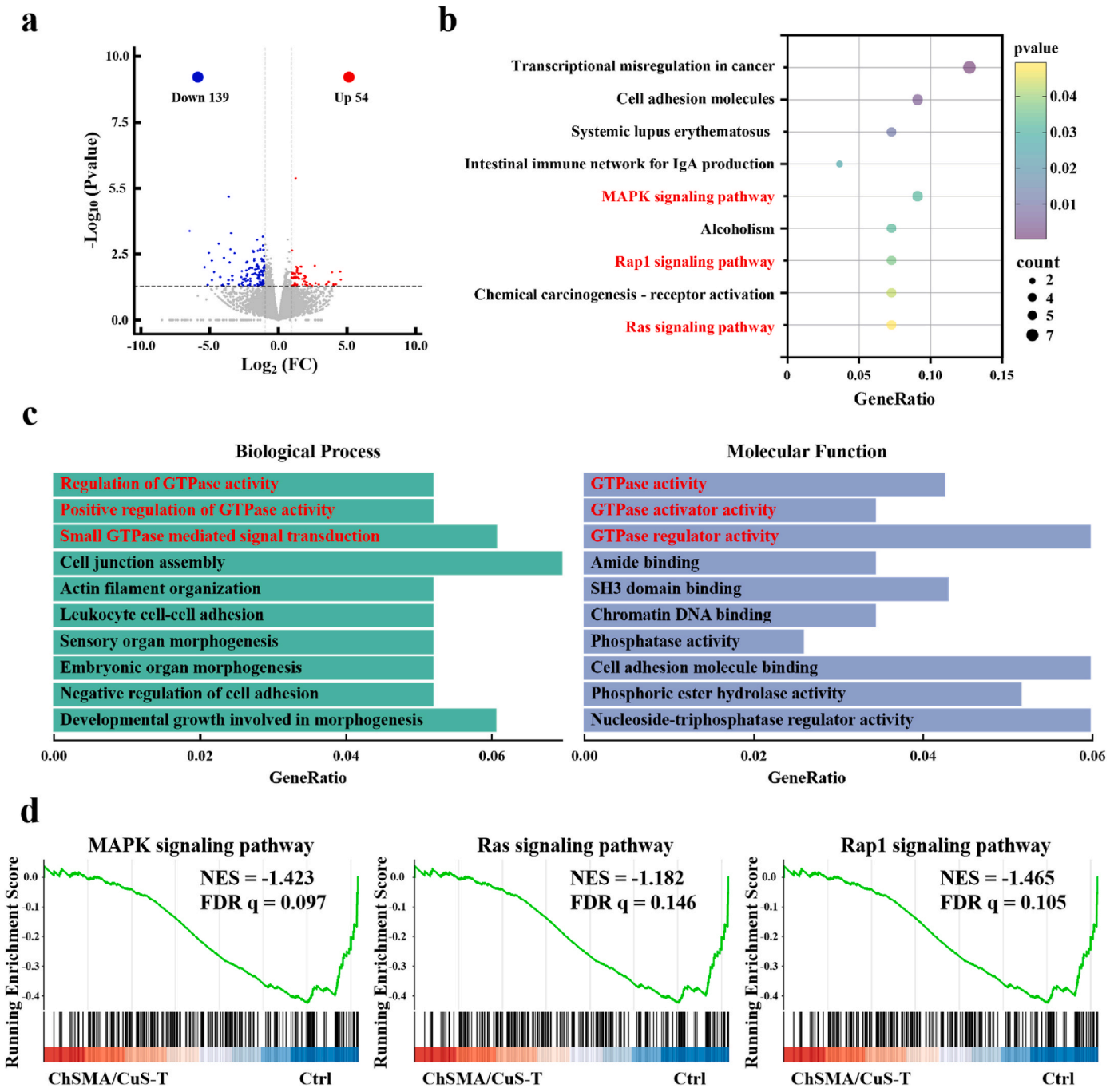

Fig. 4. Mechanism of the anti-inflammatory effect. (a) Volcano plots revealing that there were 54 up-regulated genes and 139 down-regulated genes in the comparison of the ChSMA/CuS-T hydrogel group with the PBS group. (b) KEGG pathway enrichment analysis showing that the MAPK, Rap1, and Ras pathways are highly related to the anti-inflammatory effect of ChSMA/CuS-T hydrogel. (c) GO analysis showing that GTPase activity is enriched within biological process and molecular functions. (d) GSEA confirming that the MAPK, Rap1, and Ras pathways are inhibited in the ChSMA/CuS-T hydrogel groups.

glycosaminoglycans (GAGs), including heparin, heparan sulfate, keratan sulfate, dermatan sulfate, and hyaluronic acid, ChS exhibits better protein encapsulation and stronger interactions with cytokines in the ECM [19]. A previous study also shows that ChS can enhance the response of MSCs to TGF-β1, thereby promoting chondrogenesis [53]. We assessed the relative expression of key chondrogenic genes, including *Col-2*, *ACAN*, and *SOX9*. SOX9 is a pivotal transcription factor in chondrocytes, which binds to HMG-box site in DNA and transactivates cartilage genes Col-2 and ACAN [54,55]. In addition, SOX9 is downregulated in senescent and dedifferentiated chondrocytes, thus the level of SOX9 can reflect process of chondrogenesis or cartilage damage [56]. Col-2 is the main structural protein of hyaline cartilage, which accounts for approximately 50 % of the dry weight of cartilage. It forms a three-dimensional by interwoven into a mesh-like structure, to provide anchoring sites for other matrix components, tensile strength, and mechanical support to cartilage [57]. ACAN is a high molecular weight proteoglycan. Its core protein is covalently bonded to a large number of chondroitin sulfate and keratan sulfate chains, forming negatively charged GAGs, which adsorb a large amount of water through osmotic pressure, endowing the ACAN aggregates with a strong water retention capacity and providing cartilage with compressive resilience. Moreover, ACAN molecule is linked to hyaluronic acid via link proteins, forming a

super-molecular complex, which further enhances the stability and compressive resistance of the ECM [58]. The solid Col-2 limits the swelling pressure from ACAN and forms the cartilage framework [59]. The *Col-2* expression of BMSCs was significantly upregulated in both the ChSMA/CuS and ChSMA/CuS-T groups, suggesting that CuS NPs, rather than ChSMA, was instrumental in promoting synthesis of Col-2. Moreover, the expression levels of *ACAN* and *SOX9* were significantly upregulated in all hydrogel groups and they were slightly higher in the ChSMA/CuS group (Fig. 5a). Subsequently, we conducted IHC staining of Col-2 and ACAN in cell pellet formed by BMSCs to further validate the long-term chondrogenesis of the hydrogels. As presented in Fig. 5b, the brown color (namely Col-2 and ACAN expression) was much deeper in all hydrogel groups compared to the control group. Specifically, cell pellets of the ChSMA/CuS and ChSMA/CuS-T groups presented significantly higher Col-2 and ACAN expressions compared with the control group (Fig. 5c).

In the inflammatory microenvironment, stem cells undergo abnormal differentiation and chondrocytes begin to transform or dedifferentiate into a fibroblastic phenotype, ultimately forming fibrocartilage with inferior mechanical properties [60]. Thus, inflammation hinders cartilage repair. The good anti-inflammatory property of ChSMA/CuS-T hydrogel motivated us to further investigate their chondrogenic inductivity under inflammation. We collected the culture supernatant of LPS-induced RAW264.7 cells and cultured BMSCs with this conditional medium to create an inflammatory microenvironment. Following a 5-day co-culture, a marked decrease in the gene expression of *Col-2*, *ACAN*, and *SOX9* was observed in BMSCs in the control group compared to the blank group, indicating that inflammatory microenvironment hampered chondrogenesis of BMSCs (Fig. 5e). ChSMA hydrogel alone also lost their chondrogenic inductivity towards BMSCs under inflammation. In contrast, BMSCs in the ChSMA/CuS-T group exhibited a significant upregulation of *Col-2* and *ACAN* compared to the control group though no significant difference was found in *SOX9* expression. These results demonstrated that the ChSMA/CuS-T hydrogel could shield BMSCs from inflammatory-mediated damage and preserve their chondrogenic inductivity even in the RA-related inflammatory microenvironment.

3.5. ChSMA/CuS-T hydrogel suppresses synovial inflammation and protect cartilage in vivo

We established an AIA mouse model to assess the in vivo therapeutic efficacy of the hydrogels because AIA model exhibited more severe joint inflammation compared to collagen-induced arthritis model [61]. The hydrogels were intra-articularly injected into the joint cavity of AIA mice every week (Fig. 6a). After 4 weeks of different treatments, we found that the hyperplasia of synovial tissue led to the formation of pannus, which invaded into the joint space and caused extensive cartilage damage in the PBS group (determined by H&E staining; Fig. 6b and c). A similar situation was also observed in the ChSMA group. Notably, in both ChSMA/CuS and ChSMA/CuS-T group, synovial invasion was mild and the integrity of the cartilage was well preserved.

Similarly, Safranine O-fast green staining (Fig. 6d and e) confirmed the full-thickness cartilage defect and severe loss of staining (namely, the loss of glycosaminoglycan), in the AIA mice treated with PBS. In contrast, the staining of cartilage (red color by Safranine O) was deepest in the ChSMA/CuS-T group. Thus, the PBS group had the highest Mankin Score and Synovitis Score, whereas the ChSMA/CuS-T hydrogel achieved the lowest scores due to their properties of inhibiting synovial invasion and enhancing chondrogenesis (Fig. 6f).

In addition, we conducted a gait analysis to study the behavioral changes of AIA mice after treatment. Ankylosis and angular deformities of joints emerge as RA progresses. By measuring parameters such as stride frequency, stride length, and the durations of stance, braking, propulsion, and swing phases, gait analysis can reflect changes in the knee joints of mice. The gait map was presented in Fig. 6h. Print positions represent the distance between the position of the hind paw and the position of the previously placed front paw on the same side of the body (ipsilateral) and in the same step cycle. The result of right hinder paw print positions showed that the ChSMA/CuS-T group had a significantly higher print positions index compared to other groups (Fig. 6g). Higher print positions index means the longest gaps between ipsilateral front and hind paws. This result indicated that the AIA mice accepted ChSMA/CuS-T treatment presented a better joint and hind movement ability. Moreover, single stance refers to the duration (in seconds) of ground contact for a single hind paw and is used for pain accessing [62,63]. We found that the single stance of right hind paw of AIA mice in the ChSMA/CuS-T group was significantly higher relative to other groups (Fig. 6g). This result indicated that the reduction of synovium hyperplasia by ChSMA/CuS-T hydrogel provided a higher flexibility of movement through reducing pain and maintaining the overall integrity of the knee joint. Previous evidence reveals that RA-FLS can enhance the growth of pain-sensing neurons in regions of synovial hypertrophy in RA [64]. Our results are also consistent with previous report that RA mouse exhibit less stance compared with healthy mouse [65]. Thus, the diminished synovial invasion of mice treated by ChSMA/CuS-T hydrogel contributed to the improved mobility and reduced pain.

To further confirm the therapeutic effect of ChSMA/CuS-T hydrogel, we performed IF staining on the joint sections after treatment (Fig. 7a and b). In the PBS group, MMP-9 was highly expressed within the synovial tissue. TNF-α was also abundant in both synovial and cartilage tissues due to synovial invasion. This was accompanied by low expression of Col-2 and ACAN in the cartilage tissue, indicating cartilage damage due to synovial inflammation. All hydrogel treatments demonstrated varying degrees of synovium inhibition and cartilage protection. Notably, in the ChSMA/CuS-T group, MMP-9 and TNF-α expressions exhibited negligible fluorescence signals in both synovium and cartilage. Moreover, the fluorescence signals of Col-2 and ACAN were highest in the ChSMA/CuS-T group, suggesting a significant restoration of cartilage integrity after ChSMA/CuS-T hydrogel treatment. These above-mentioned results demonstrated the ChSMA/CuS-T hydrogel could effectively alleviate inflammation and promote cartilage regeneration, achieving the best therapeutic effects in vivo.

3.6. ChSMA/CuS-T hydrogel is biocompatible in vivo

Finally, the biosafety of the hydrogels in vivo was investigated. After treatment, H&E staining (Fig. 8a) of main organs of mice showed that the heart cardiac circular and longitudinal muscles had intact structure. Liver portal areas and hepatocytes exhibited no acute or chronic damage, such as cell swelling, cell content leakage, nuclear disintegration, or massive infiltration of inflammatory cells. Spleen splenic capsule trabeculae and splenic corpuscles were normal without hemolysis. Lung pulmonary alveoli and airway epithelium displayed no inflammatory exudation. The kidney renal cortex and medulla indicated normal form. Furthermore, the key indexes of liver functions, including aspartate aminotransferase (AST) and alanine aminotransferase (ALT), as well as kidney functions, including serum creatinine (SCr) and serum uric acid (SUA) were detected by blood biochemistry test (Fig. 8b). All these markers were within the normal range across all groups. Hence, the intra-articular administration of ChSMA/CuS-T hydrogel did not cause systemic toxicity and any undesired side-effects.

4. Conclusion

In sum, we prepared a new injectable hydrogel that integrated the ECM-mimic ChSMA hydrogel with MMP-9-binding peptide-functionalized CuS NPs. Our results demonstrated that the integration of CuS NPs into the hydrogel could inhibit the migration and invasion of RA-FLS, exert the anti-inflammatory effects on M1 type macrophages, and enhance the chondrogenic inductivity towards BMSCs even under

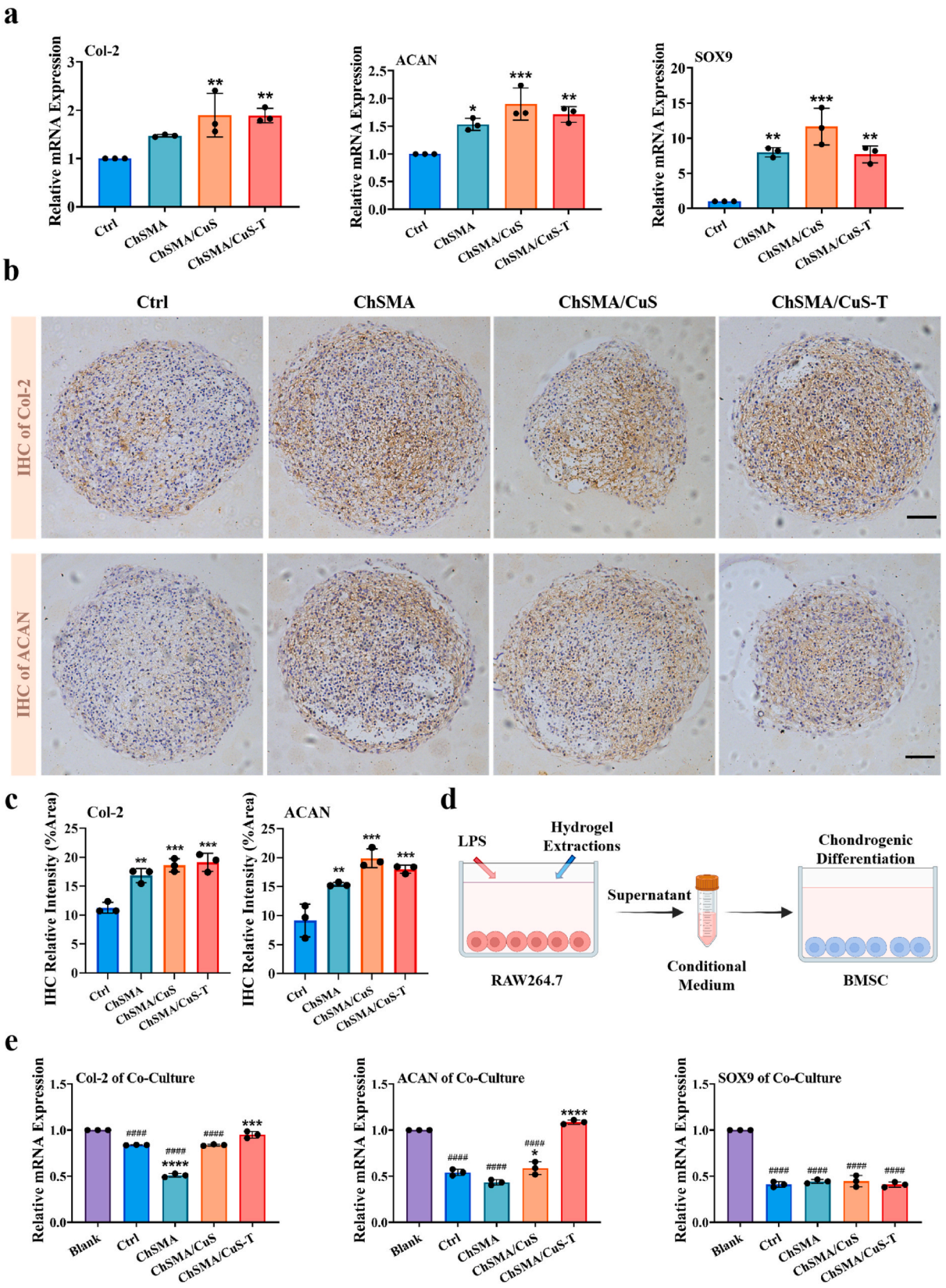

Fig. 5. Chondroinductivity of the hydrogels. (a) Relative gene expression levels of *Col-2*, *ACAN* and *SOX9* of BMSCs in different groups. (b) Immunohistochemistry staining of Col-2 and ACAN expressions in cell pellets. Scale bar = 100 μm. (c) Statistical analysis of Col-2 and ACAN expressions derived from the immunohistochemistry staining of cell pellets. (d) Illustration of the chondroninduction study of BMSCs under inflammatory microenvironment. The culture supernatant of M1 type macrophages were mixed with different hydrogels extracts to obtain the conditional media. (e) Relative gene expression levels of *Col-2*, *ACAN* and *SOX9* of BMSCs after cocultured with different conditional media. These results indicated that ChSMA/CuS-T hydrogel could promote the chondrogenic differentiation of BMSCs even under inflammatory microenvironment. $^{*}P < 0.05$, $^{**}P < 0.01$, $^{***}P < 0.001$, $^{****}P < 0.0001$, compared with the control group. $^{\#\#\#\#}P < 0.0001$, compared with the blank group.

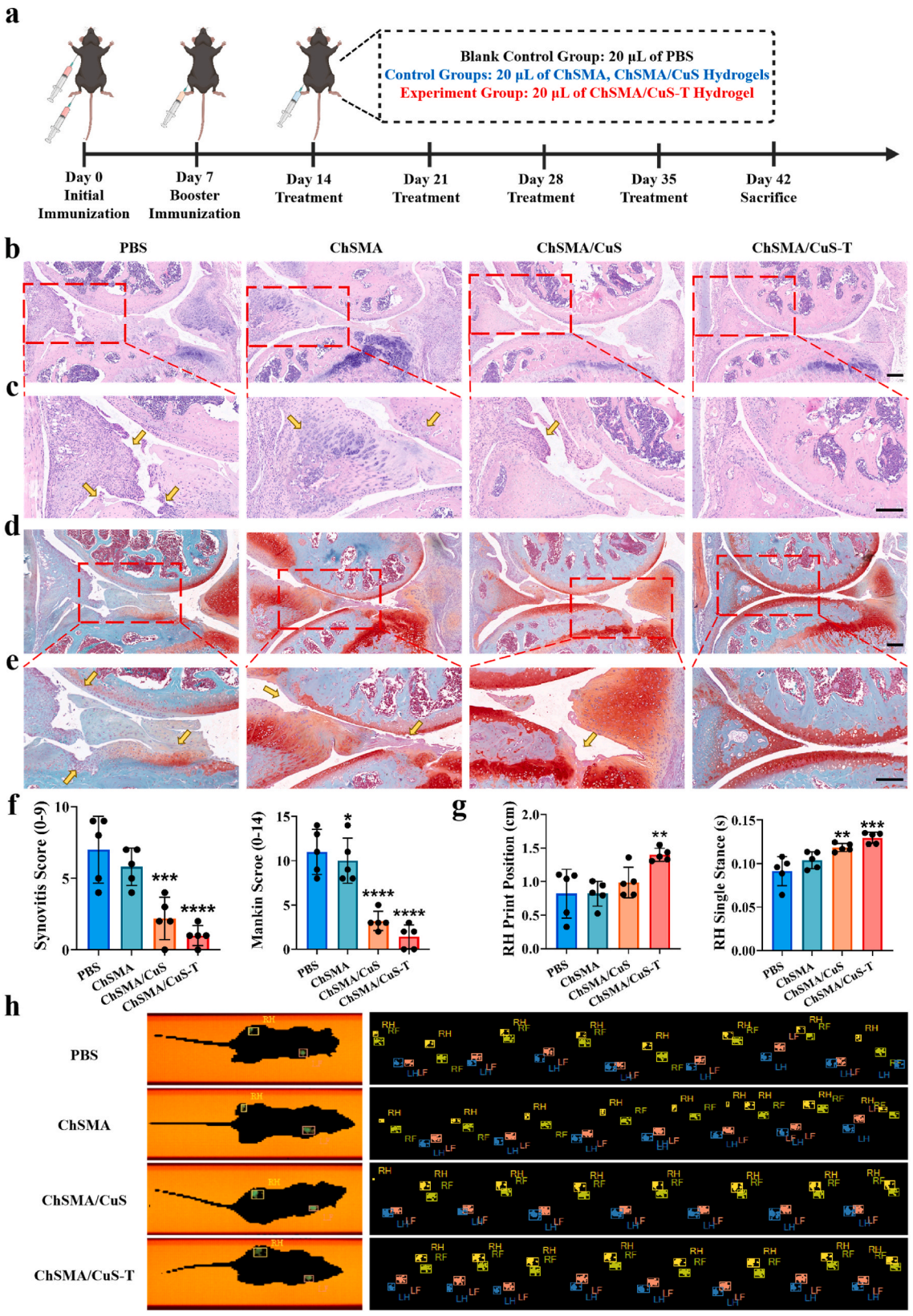

Fig. 6. Therapeutic effect of the hydrogels on AIA mice. (a) Illustration of establishment of AIA mice and treatment design. (b, c) Representative H&E staining of the knee joints of AIA mice after different treatments. Synovial invasion was highlight by yellow arrows. Scale bar = 200 μm. (d, e) Safranine O-fast green staining of the knee joints. Cartilage destruction was highlight by yellow arrows. Scale bar = 200 μm. (f) Histological evaluation of knee joint sections using Synovitis score and Mankin score. (g) Statistical analysis of gait analysis of AIA mice after treatment. (h) Representative gait diagram of mice in different groups. RH = right hind paw, LH = left hind paw, RF = right front paw, LF = left front paw. These results indicated that ChSMA/CuS-T hydrogel exhibited the best therapeutic effects on AIA mice among all groups. *$P < 0.05$, **$P < 0.01$, ***$P < 0.001$, ****$P < 0.0001$ compared with the PBS group. (For interpretation of the references to color in this figure legend, the reader is referred to the Web version of this article.)

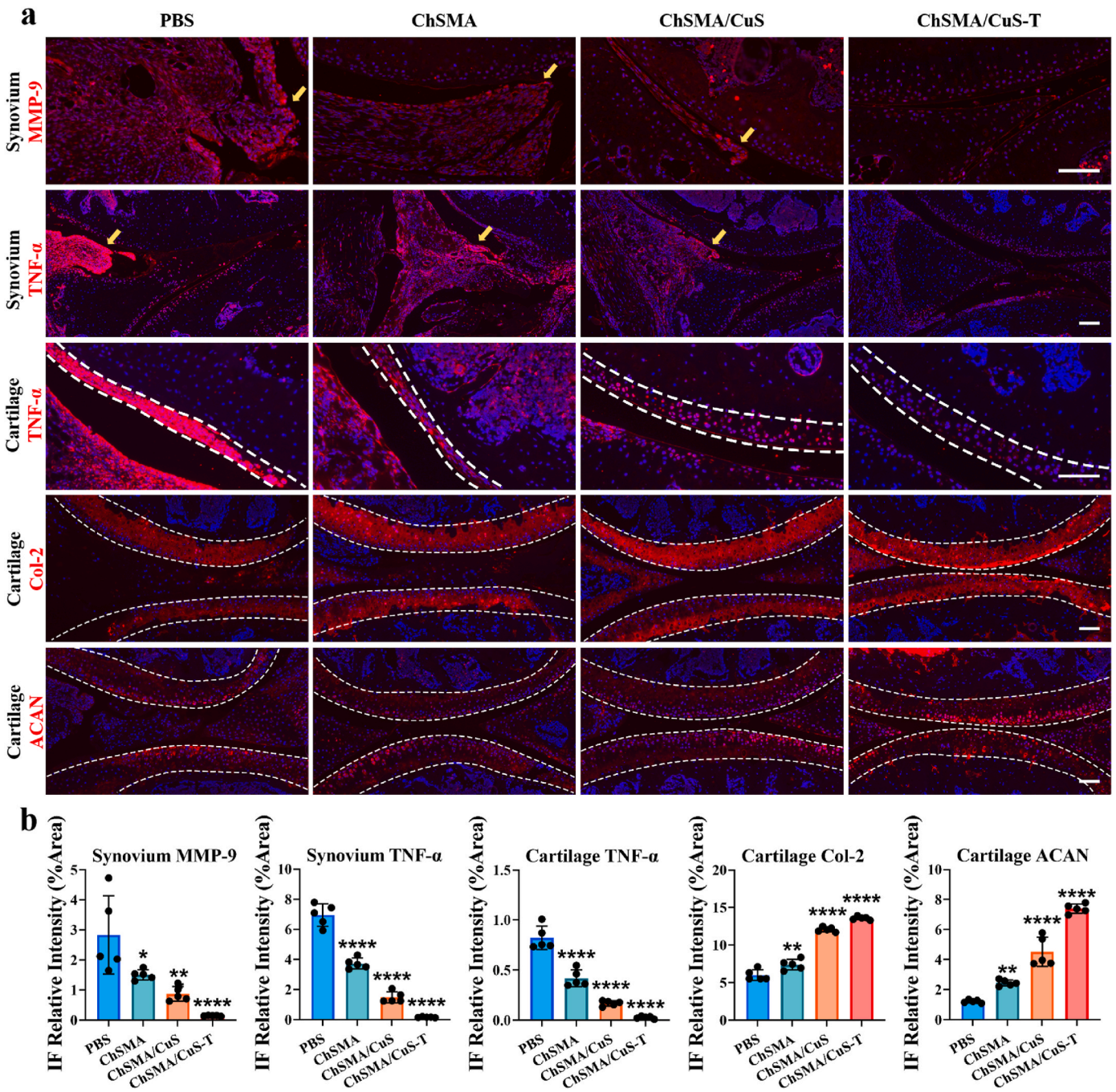

Fig. 7. Immunofluorescence staining of knee joints. (a) MMP-9 expression in synovial tissue, TNF-α synovium in synovial tissue and cartilage, and Col-2 and ACAN expressions in cartilage. (b) Statistical analysis of immunofluorescence intensity derived from panel (a). The yellow arrows show the areas of synovium invasion and the dotted white lines showed the cartilage area in knee joint. These results indicated that ChSMA/CuS-T hydrogel could inhibit MMP-9 and TNF-α expressions while promoting cartilage repair under inflammatory microenvironment. Scale bar = 100 μm *$P < 0.05$, **$P < 0.01$, ***$P < 0.001$, ****$P < 0.0001$, compared with the PBS group. (For interpretation of the references to color in this figure legend, the reader is referred to the Web version of this article.)

inflammatory conditions. These effects were further boosted when CuS NPs were modified with the MMP-9-binding peptide (CuS-T). Subsequently, the intra-articular injection of ChSMA/CuS-T hydrogel successfully inhibited synovial inflammation and promoted cartilage repair in an AIA mouse model without causing any side-effects. Thus, our study offered a potentially safe and efficient treatment approach for RA.

CRediT authorship contribution statement

Zhanpeng Xue: Writing – original draft, Visualization, Methodology, Investigation. **Nan Li:** Methodology, Investigation. **Kaijun Du:** Methodology, Investigation. **Jianxiong Shu:** Methodology, Investigation. **Zhenwen Huang:** Methodology, Investigation. **Zhifei Gao:** Validation, Methodology. **Xiaobo Xie:** Supervision, Resources, Methodology, Conceptualization. **Qi Li:** Writing – review & editing, Supervision, Funding acquisition, Conceptualization. **Yao Lu:** Writing – review & editing, Supervision, Funding acquisition, Conceptualization.

Declaration of competing interest

The authors declare that they have no known competing financial interests or personal relationships that could have appeared to influence

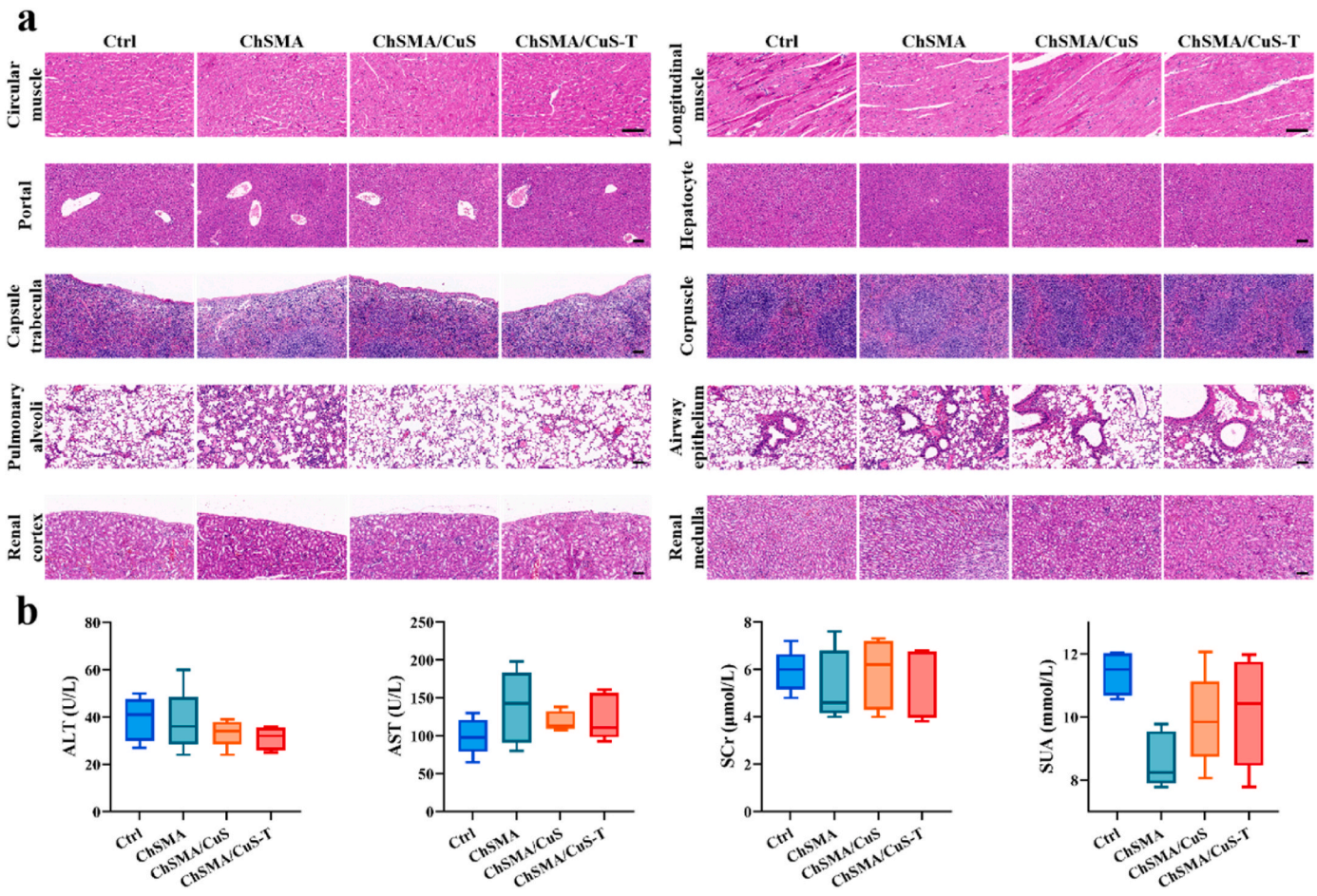

Fig. 8. In vivo safety of hydrogels. (a) H&E staining of the main organs after treatments, including heart, liver, spleen, and lung. All organs presented normal morphology. Scale bar = 100 μm. (b) Serum ALT, AST, Cr, and UA levels of mice were within the normal range, indicating that ChSMA/CuS-T hydrogel did not cause any undesired effects on liver and kidney functions.

the work reported in this paper.

Acknowledgements

This study was supported by the National Natural Science Foundation of China (No. 82172391) and Guangdong Basic and Applied Basic Research foundation (No. 2024B1515020015).

Appendix A. Supplementary data

Supplementary data to this article can be found online at https://doi.org/10.1016/j.mtbio.2025.101792.

Data availability

Data will be made available on request.

References

[1] S. Alivernini, G.S. Firestein, I.B. McInnes, The pathogenesis of rheumatoid arthritis, Immunity 55 (2022) 2255–2270, https://doi.org/10.1016/j.immuni.2022.11.009.
[2] L.G.N. De Almeida, H. Thode, Y. Eslambolchi, S. Chopra, D. Young, S. Gill, L. Devel, A. Dufour, Matrix Metalloproteinases, From molecular mechanisms to physiology, pathophysiology, and pharmacology, Pharmacol. Rev. 74 (2022) 714–770, https://doi.org/10.1124/pharmrev.121.000349.
[3] M. Xue, K. McKelvey, K. Shen, N. Minhas, L. March, S.-Y. Park, C.J. Jackson, Endogenous MMP-9 and not MMP-2 promotes rheumatoid synovial fibroblast survival, inflammation and cartilage degradation, Rheumatology 53 (2014) 2270–2279, https://doi.org/10.1093/rheumatology/keu254.
[4] M. Cutolo, R. Campitiello, E. Gotelli, S. Soldano, The role of M1/M2 macrophage polarization in rheumatoid arthritis synovitis, Front. Immunol. 13 (2022) 867260, https://doi.org/10.3389/fimmu.2022.867260.
[5] P. Zhang, C. Wu, X. Huang, C. Shen, L. Li, W. Zhang, C. Yao, Aspirin suppresses TNF-α-induced MMP-9 expression via NF-κB and MAPK signaling pathways in RAW264.7 cells, Exp. Ther. Med. 14 (2017) 5597–5604, https://doi.org/10.3892/etm.2017.5252.
[6] Y. Bian, Z. Xiang, Y. Wang, Q. Ren, G. Chen, B. Xiang, J. Wang, C. Zhang, S. Pei, S. Guo, L. Xiao, Immunomodulatory roles of metalloproteinases in rheumatoid arthritis, Front. Pharmacol. 14 (2023) 1285455, https://doi.org/10.3389/fphar.2023.1285455.
[7] M. Ferrari, S.C. Onuoha, L. Fossati-Jimack, A. Nerviani, P.L. Alves, S. Pagani, C. Deantonio, F. Colombo, C. Santoro, D. Sblattero, C. Pitzalis, Novel bispecific antibody for synovial-specific target delivery of anti-TNF therapy in rheumatoid arthritis, Front. Immunol. 12 (2021) 640070, https://doi.org/10.3389/fimmu.2021.640070.
[8] D.P.C. De Rooy, A. Zhernakova, R. Tsonaka, A. Willemze, B.A.S. Kurreeman, G. Trynka, L. Van Toorn, R.E.M. Toes, T.W.J. Huizinga, J.J. Houwing-Duistermaat, P.K. Gregersen, A.H.M. Van Der Helm-van Mil, A genetic variant in the region of *MMP-9* is associated with serum levels and progression of joint damage in rheumatoid arthritis, Ann. Rheum. Dis. 73 (2014) 1163–1169, https://doi.org/10.1136/annrheumdis-2013-203375.
[9] Z.A. Rashid, S.K. Bardaweel, Novel matrix metalloproteinase-9 (MMP-9) inhibitors in cancer treatment, Int. J. Mol. Sci. 24 (2023) 12133, https://doi.org/10.3390/ijms241512133.
[10] S. Das, S.A. Amin, T. Jha, Inhibitors of gelatinases (MMP-2 and MMP-9) for the management of hematological malignancies, Eur. J. Med. Chem. 223 (2021) 113623, https://doi.org/10.1016/j.ejmech.2021.113623.
[11] S. Mondal, N. Adhikari, S. Banerjee, S.A. Amin, T. Jha, Matrix metalloproteinase-9 (MMP-9) and its inhibitors in cancer: a minireview, Eur. J. Med. Chem. 194 (2020) 112260, https://doi.org/10.1016/j.ejmech.2020.112260.
[12] B. Grillet, R.V.S. Pereira, J. Van Damme, A. Abu El-Asrar, P. Proost, G. Opdenakker, Matrix metalloproteinases in arthritis: towards precision medicine, Nat. Rev. Rheumatol. 19 (2023) 363–377, https://doi.org/10.1038/s41584-023-00966-w.

[13] L. Autelitano, M.C. Meazzini, Alveolar cleft reconstruction with vomerine bone: two surgical procedures in one step: a case series, Plast, Aesthetic Res. 10 (2023) 17, https://doi.org/10.20517/2347-9264.2022.57.
[14] J.-W. Choi, Y.-C. Kim, Asian facial recontouring surgery, Plast. Aesthetic Res. 10 (2023) 59, https://doi.org/10.20517/2347-9264.2023.30.
[15] I.A. Jones, R. Togashi, M.L. Wilson, N. Heckmann, C.T. Vangsness, Intra-articular treatment options for knee osteoarthritis, Nat. Rev. Rheumatol. 15 (2019) 77–90, https://doi.org/10.1038/s41584-018-0123-4.
[16] M.C. Bruno, M.C. Cristiano, C. Celia, N. d'Avanzo, A. Mancuso, D. Paolino, J. Wolfram, M. Fresta, Injectable drug delivery systems for osteoarthritis and rheumatoid arthritis, ACS Nano 16 (2022) 19665–19690, https://doi.org/10.1021/acsnano.2c06393.
[17] T. Saeedi, H.F. Alotaibi, P. Prokopovich, Polymer colloids as drug delivery systems for the treatment of arthritis, Adv. Colloid Interface Sci. 285 (2020) 102273, https://doi.org/10.1016/j.cis.2020.102273.
[18] J. Lu, Z. Gao, W. He, Y. Lu, Harnessing the potential of hyaluronic acid methacrylate (HAMA) hydrogel for clinical applications in orthopaedic diseases, J. Orthop. Transl. 50 (2025) 111–128, https://doi.org/10.1016/j.jot.2024.11.004.
[19] CarlC.L. Schuurmans, M. Mihajlovic, C. Hiemstra, K. Ito, W.E. Hennink, T. Vermonden, Hyaluronic acid and chondroitin sulfate (meth)acrylate-based hydrogels for tissue engineering: synthesis, characteristics and pre-clinical evaluation, Biomaterials 268 (2021) 120602, https://doi.org/10.1016/j.biomaterials.2020.120602.
[20] J. Yang, M. Shen, H. Wen, Y. Luo, R. Huang, L. Rong, J. Xie, Recent advance in delivery system and tissue engineering applications of chondroitin sulfate, Carbohydr. Polym. 230 (2020) 115650, https://doi.org/10.1016/j.carbpol.2019.115650.
[21] P. Xiao, X. Han, Y. Huang, J. Yang, L. Chen, Z. Cai, N. Hu, W. Cui, W. Huang, Reprogramming macrophages via immune cell mobilized hydrogel microspheres for osteoarthritis treatments, Bioact. Mater. 32 (2024) 242–259, https://doi.org/10.1016/j.bioactmat.2023.09.010.
[22] Y. He, M. Sun, J. Wang, X. Yang, C. Lin, L. Ge, C. Ying, K. Xu, A. Liu, L. Wu, Chondroitin sulfate microspheres anchored with drug-loaded liposomes play a dual antioxidant role in the treatment of osteoarthritis, Acta Biomater. 151 (2022) 512–527, https://doi.org/10.1016/j.actbio.2022.07.052.
[23] K. Miao, Y. Zhou, X. He, Y. Xu, X. Zhang, H. Zhao, X. Zhou, Q. Gu, H. Yang, X. Liu, L. Huang, Q. Shi, Microenvironment-responsive bilayer hydrogel microspheres with gelatin-shell for osteoarthritis treatment, Int. J. Biol. Macromol. 261 (2024) 129862, https://doi.org/10.1016/j.ijbiomac.2024.129862.
[24] Y. Xu, Q. Saiding, X. Zhou, J. Wang, W. Cui, X. Chen, Electrospun fiber-based immune engineering in regenerative medicine, Smart Med 3 (2024) e20230034, https://doi.org/10.1002/SMMD.20230034.
[25] Y. Lei, Q. Zhang, G. Kuang, X. Wang, Q. Fan, F. Ye, Functional biomaterials for osteoarthritis treatment: from research to application, Smart Med 1 (2022) e20220014, https://doi.org/10.1002/SMMD.20220014.
[26] Y. Cai, C. Wu, Q. Ou, M. Zeng, S. Xue, J. Chen, Y. Lu, C. Ding, Enhanced osteoarthritis therapy by nanoengineered mesenchymal stem cells using biomimetic CuS nanoparticles loaded with plasmid DNA encoding TGF-β1, Bioact. Mater. 19 (2023) 444–457, https://doi.org/10.1016/j.bioactmat.2022.04.021.
[27] X. Wang, Y. Cai, C. Wu, J. Liang, K. Tang, Z. Lin, L. Chen, Y. Lu, Q. Wang, Conversion of Senescent Cartilage into a Pro-chondrogenic Microenvironment with Antibody-Functionalized Copper Sulfate Nanoparticles for Efficient Osteoarthritis Therapy, vol. 21, 2023, p. 258, https://doi.org/10.1186/s12951-023-02036-5.
[28] Y. Lu, J. Chen, L. Li, Y. Cao, Y. Zhao, X. Nie, C. Ding, Hierarchical functional nanoparticles boost osteoarthritis therapy by utilizing joint-resident mesenchymal stem cells, J. Nanobiotechnol. 20 (2022) 89, https://doi.org/10.1186/s12951-022-01297-w.
[29] C. Wu, Z. Huang, J. Chen, N. Li, Y. Cai, J. Chen, G. Ruan, W. Han, C. Ding, Y. Lu, Efficiently directing differentiation and homing of mesenchymal stem cells to boost cartilage repair in osteoarthritis via a nanoparticle and peptide dual-engineering strategy, Biomaterials 312 (2025) 122720, https://doi.org/10.1016/j.biomaterials.2024.122720.
[30] E. Koivunen, W. Arap, H. Valtanen, A. Rainisalo, O.P. Medina, P. Heikkilä, C. Kantor, C.G. Gahmberg, T. Salo, Y.T. Konttinen, T. Sorsa, E. Ruoslahti, R. Pasqualini, Tumor targeting with a selective gelatinase inhibitor, Nat. Biotechnol. 17 (1999) 768–774, https://doi.org/10.1038/11703.
[31] H.K. Cheung, T.T.Y. Han, D.M. Marecak, J.F. Watkins, B.G. Amsden, L.E. Flynn, Composite hydrogel scaffolds incorporating decellularized adipose tissue for soft tissue engineering with adipose-derived stem cells, Biomaterials 35 (2014) 1914–1923, https://doi.org/10.1016/j.biomaterials.2013.11.067.
[32] H. Chen, W. Wang, Y. Yang, B. Zhang, Z. Li, L. Chen, Q. Tu, T. Zhang, D. Lin, H. Yi, H. Xia, Y. Lu, A sequential stimuli-responsive hydrogel promotes structural and functional recovery of severe spinal cord injury, Biomaterials 316 (2025) 122995, https://doi.org/10.1016/j.biomaterials.2024.122995.
[33] H. Liao, W. Qi, Z. Xue, K. Wu, L. Jiang, C. Wu, Z. Huang, Q. Li, Y. Lu, A multifunctional supramolecular hydrogel that rapidly binds TNF-α for efficient reduction of synovial inflammation and cartilage destruction in rheumatoid arthritis, Chem. Eng. J. 477 (2023) 147125, https://doi.org/10.1016/j.cej.2023.147125.
[34] Q. Chen, K. Fan, G. Song, X. Wang, J. Zhang, H. Chen, X. Qin, Y. Lu, W. Qi, Rapamycin regulates osteogenic differentiation through Parkin-mediated mitophagy in rheumatoid arthritis, Int. Immunopharmacol. 113 (2022) 109407, https://doi.org/10.1016/j.intimp.2022.109407.
[35] B. Grillet, K. Yu, E. Ugarte-Berzal, R. Janssens, R.V.S. Pereira, L. Boon, E. Martens, N. Berghmans, I. Ronsse, I. Van Aelst, P. Fiten, R. Conings, J. Vandooren, P. Verschueren, J. Van Damme, P. Proost, G. Opdenakker, Proteoform analysis of matrix metalloproteinase-9/gelatinase B and discovery of its citrullination in rheumatoid arthritis synovial fluids, Front. Immunol. 12 (2021) 763832, https://doi.org/10.3389/fimmu.2021.763832.
[36] S.K. Stojanovic, B.N. Stamenkovic, J.M. Cvetkovic, V.G. Zivkovic, M.R. A. Apostolovic, Matrix metalloproteinase-9 level in synovial fluid—association with joint destruction in early rheumatoid arthritis, Medicina (Mex.) 59 (2023) 167, https://doi.org/10.3390/medicina59010167.
[37] G. Nygaard, G.S. Firestein, Restoring synovial homeostasis in rheumatoid arthritis by targeting fibroblast-like synoviocytes, Nat. Rev. Rheumatol. 16 (2020) 316–333, https://doi.org/10.1038/s41584-020-0413-5.
[38] F. Zhang, A.H. Jonsson, A. Nathan, N. Millard, M. Curtis, Q. Xiao, M. Gutierrez-Arcelus, W. Apruzzese, G.F.M. Watts, D. Weisenfeld, S. Nayar, J. Rangel-Moreno, N. Meednu, K.E. Marks, I. Mantel, J.B. Kang, L. Rumker, J. Mears, K. Slowikowski, K. Weinand, D.E. Orange, L. Geraldino-Pardilla, K.D. Deane, D. Tabechian, A. Ceponis, G.S. Firestein, M. Maybury, I. Sahbudin, A. Ben-Artzi, A.M. Mandelin, A. Nerviani, M.J. Lewis, F. Rivellese, C. Pitzalis, L.B. Hughes, D. Horowitz, E. DiCarlo, E.M. Gravallese, B.F. Boyce, J. Albrecht, J.L. Barnas, J.M. Bathon, D. L. Boyle, S.L. Bridges, D. Campbell, H.L. Carr, A. Chicoine, A. Cordle, P. Dunn, L. Forbess, P.K. Gregersen, J.M. Guthridge, L.B. Ivashkiv, K. Ishigaki, J.A. James, G. Keras, I. Korsunsky, A. Lakhanpal, J.A. Lederer, Z.J. Li, Y. Li, A. McDavid, M. J. McGeachy, K. Raza, Y. Reshef, C. Ritchlin, W.H. Robinson, S. Sakaue, J. A. Seifert, A. Singaraju, M.H. Smith, D. Scheel-Toellner, P.J. Utz, M.H. Weisman, A. Wyse, Z. Zhu, L.W. Moreland, S.M. Goodman, H. Perlman, V.M. Holers, K. P. Liao, A. Filer, V.P. Bykerk, K. Wei, D.A. Rao, L.T. Donlin, J.H. Anolik, M. B. Brenner, S. Raychaudhuri, Accelerating Medicines Partnership: RA/SLE Network, Deconstruction of rheumatoid arthritis synovium defines inflammatory subtypes, Nature 623 (2023) 616–624, https://doi.org/10.1038/s41586-023-06708-y.
[39] W. Liu, C. Wu, Q. Wang, L. Kuang, A. Le, Tanshinone IIA relieves arthritis by inhibiting autophagy of fibroblast-like synoviocytes via matrix metalloproteinase9/receptor for advanced glycation end product/toll-like receptor 9 signal axis in mice with collagen-induced arthritis, Phytother Res. 37 (2023) 1391–1404, https://doi.org/10.1002/ptr.7748.
[40] Y. Shi, Q. Wu, W. Xuan, X. Feng, F. Wang, B.P. Tsao, M. Zhang, W. Tan, Transcription factor SOX5 promotes the migration and invasion of fibroblast-like synoviocytes in part by regulating MMP-9 expression in collagen-induced arthritis, Front. Immunol. 9 (2018) 749, https://doi.org/10.3389/fimmu.2018.00749.
[41] S. Lu, H. Jang, S. Muratcioglu, A. Gursoy, O. Keskin, R. Nussinov, J. Zhang, Ras conformational ensembles, allostery, and signaling, Chem. Rev. 116 (2016) 6607–6665, https://doi.org/10.1021/acs.chemrev.5b00542.
[42] C. Korzeniecki, R. Priefer, Targeting KRAS mutant cancers by preventing signaling transduction in the MAPK pathway, Eur. J. Med. Chem. 211 (2021) 113006, https://doi.org/10.1016/j.ejmech.2020.113006.
[43] Y. Wu, Z. Wang, Y. Ge, Y. Zhu, T. Tian, J. Wei, Y. Jin, Y. Zhao, Q. Jia, J. Wu, L. Ge, Microenvironment responsive hydrogel exerting inhibition of cascade immune activation and elimination of synovial fibroblasts for rheumatoid arthritis therapy, J. Contr. Release 370 (2024) 747–762, https://doi.org/10.1016/j.jconrel.2024.05.021.
[44] S. Liu, H. Ma, H. Zhang, C. Deng, P. Xin, Recent advances on signaling pathways and their inhibitors in rheumatoid arthritis, Clin. Immunol. 230 (2021) 108793, https://doi.org/10.1016/j.clim.2021.108793.
[45] V. Paunovic, M.M. Harnett, Mitogen-activated protein kinases as therapeutic targets for rheumatoid arthritis, Drugs 73 (2013) 101–115, https://doi.org/10.1007/s40265-013-0014-6.
[46] M. Sadeghi Shaker, M. Rokni, M. Mahmoudi, E. Farhadi, Ras family signaling pathway in immunopathogenesis of inflammatory rheumatic diseases, Front. Immunol. 14 (2023) 1151246, https://doi.org/10.3389/fimmu.2023.1151246.
[47] Y. Song, Z. Bi, Y. Liu, F. Qin, Y. Wei, X. Wei, Targeting RAS–RAF–MEK–ERK signaling pathway in human cancer: current status in clinical trials, Genes Dis 10 (2023) 76–88, https://doi.org/10.1016/j.gendis.2022.05.006.
[48] E. Caron, Cellular functions of the Rap1 GTP-binding protein: a pattern emerges, J. Cell Sci. 116 (2003) 435–440, https://doi.org/10.1242/jcs.00238.
[49] S. Shah, E.J. Brock, K. Ji, R.R. Mattingly, Ras and Rap1: a tale of two GTPases, Semin. Cancer Biol. 54 (2019) 29–39, https://doi.org/10.1016/j.semcancer.2018.03.005.
[50] Y. Wang, C. Han, D. Cui, Y. Li, Y. Ma, W. Wei, Is macrophage polarization important in rheumatoid arthritis? Int. Immunopharmacol. 50 (2017) 345–352, https://doi.org/10.1016/j.intimp.2017.07.019.
[51] S.-S. Nah, H.-J. Won, E. Ha, I. Kang, H.Y. Cho, S.-J. Hur, S.-H. Lee, H.H. Baik, Epidermal growth factor increases prostaglandin E2 production via ERK1/2 MAPK and NF-κB pathway in fibroblast like synoviocytes from patients with rheumatoid arthritis, Rheumatol. Int. 30 (2010) 443–449, https://doi.org/10.1007/s00296-009-0976-6.
[52] Crosstalk between synovial macrophages and fibroblasts in rheumatoid arthritis, Histol. Histopathol. 38 (2023) 1231–1238, https://doi.org/10.14670/HH-18-628.
[53] J.J. Lim, J.S. Temenoff, The effect of desulfation of chondroitin sulfate on interactions with positively charged growth factors and upregulation of cartilaginous markers in encapsulated MSCs, Biomaterials 34 (2013) 5007–5018, https://doi.org/10.1016/j.biomaterials.2013.03.037.
[54] H. Song, K.-H. Park, Regulation and function of SOX9 during cartilage development and regeneration, Semin. Cancer Biol. 67 (2020) 12–23, https://doi.org/10.1016/j.semcancer.2020.04.008.
[55] V. Lefebvre, M. Angelozzi, A. Haseeb, SOX9 in cartilage development and disease, Curr. Opin. Cell Biol. 61 (2019) 39–47, https://doi.org/10.1016/j.ceb.2019.07.008.

[56] S. Ashraf, B.-H. Cha, J.-S. Kim, J. Ahn, I. Han, H. Park, S.-H. Lee, Regulation of senescence associated signaling mechanisms in chondrocytes for cartilage tissue regeneration, Osteoarthr. Cartil. 24 (2016) 196–205, https://doi.org/10.1016/j.joca.2015.07.008.

[57] T. Batsalova, B. Dzhambazov, Significance of type II collagen posttranslational modifications: from autoantigenesis to improved diagnosis and treatment of rheumatoid arthritis, Int. J. Mol. Sci. 24 (2023) 9884, https://doi.org/10.3390/ijms24129884.

[58] A.J. Hayes, J. Melrose, Aggrecan, the primary weight-bearing cartilage proteoglycan, has context-dependent, cell-directive properties in embryonic development and neurogenesis: aggrecan glycan side chain modifications convey interactive biodiversity, Biomolecules 10 (2020) 1244, https://doi.org/10.3390/biom10091244.

[59] Z. Peng, H. Sun, V. Bunpetch, Y. Koh, Y. Wen, D. Wu, H. Ouyang, The regulation of cartilage extracellular matrix homeostasis in joint cartilage degeneration and regeneration, Biomaterials 268 (2021) 120555, https://doi.org/10.1016/j.biomaterials.2020.120555.

[60] M. Li, H. Yin, Z. Yan, H. Li, J. Wu, Y. Wang, F. Wei, G. Tian, C. Ning, H. Li, C. Gao, L. Fu, S. Jiang, M. Chen, X. Sui, S. Liu, Z. Chen, Q. Guo, The immune microenvironment in cartilage injury and repair, Acta Biomater. 140 (2022) 23–42, https://doi.org/10.1016/j.actbio.2021.12.006.

[61] B. Bolon, M. Stolina, C. King, S. Middleton, J. Gasser, D. Zack, U. Feige, Rodent preclinical models for developing novel antiarthritic molecules: comparative biology and preferred methods for evaluating efficacy, BioMed Res. Int. 2011 (2011) 569068, https://doi.org/10.1155/2011/569068.

[62] P. Coulthard, S.U. Simjee, B.J. Pleuvry, Gait analysis as a correlate of pain induced by carrageenan intraplantar injection, J. Neurosci. Methods 128 (2003) 95–102, https://doi.org/10.1016/S0165-0270(03)00154-7.

[63] P. Coulthard, B.J. Pleuvry, M. Brewster, K.L. Wilson, T.V. Macfarlane, Gait analysis as an objective measure in a chronic pain model, J. Neurosci. Methods 116 (2002) 197–213, https://doi.org/10.1016/S0165-0270(02)00042-0.

[64] Z. Bai, N. Bartelo, M. Aslam, E.A. Murphy, C.R. Hale, N.E. Blachere, S. Parveen, E. Spolaore, E. DiCarlo, E.M. Gravallese, M.H. Smith, M.O. Frank, C.S. Jiang, H. Zhang, C. Pyrgaki, M.J. Lewis, S. Sikandar, C. Pitzalis, J.B. Lesnak, K. Mazhar, T. J. Price, A.-M. Malfait, R.E. Miller, F. Zhang, S. Goodman, R.B. Darnell, F. Wang, D. E. Orange, J. Albrecht, J.H. Anolik, W. Apruzzese, B.F. Boyce, D.L. Boyle, M. B. Brenner, S.L. Bridges, C.D. Buckley, J.H. Buckner, V.P. Bykerk, J. Dolan, L. T. Donlin, A. Filer, G.S. Firestein, C.Y. Fonseka, P.K. Gregersen, J.M. Guthridge, M. Gutierrez-Arcelus, V.M. Holers, L.B. Hughes, L.B. Ivashkiv, E.A. James, J. A. James, A.H. Jonsson, S. Kelly, J.A. Lederer, Y.C. Lee, A.M. Mandelin, M. J. McGeachy, J.R. Mears, N. Meednu, L. Moreland, H. Perlman, J. Rangel-Moreno, D.A. Rao, S. Raychaudhuri, C. Ritchlin, W.H. Robinson, M. Rohani-Pichavant, J. Seifert, K. Slowikowski, D. Tabechian, P.J. Utz, G.F.M. Watts, K. Wei, Accelerating Medicines Partnership RA/SLE Network, Synovial fibroblast gene expression is associated with sensory nerve growth and pain in rheumatoid arthritis, Sci. Transl. Med. 16 (2024) eadk3506, https://doi.org/10.1126/scitranslmed.adk3506.

[65] J. Bao, Y. Song, M. Hang, H. Xu, Q. Li, P. Wang, T. Chen, M. Xia, Q. Shi, Y. Wang, X. Wang, Q. Liang, Huangqi Guizhi Wuwu Decoction suppresses inflammation and bone destruction in collagen-induced arthritis mice, Chin. Herb. Med. 16 (2024) 274–281, https://doi.org/10.1016/j.chmed.2023.10.003.